

STEADY-STATE MODEL OF NEUTRON STAR
CRUST

Hugo Olivares

Department of Physics

McGill University

June 2008

A thesis submitted to McGill University in partial fulfillment of the
requirements of the degree of Master of Science.

©Hugo Olivares 2008

Contents

Acknowledgements	v
Abstract	vii
Abrégé	ix
1 Luminosity phenomena in neutron stars	1
§1.1 Cooling of isolated neutron stars	1
§1.2 X-ray Burst in Binary Systems	4
§1.2.1 Overall features	4
§1.2.2 Optical Observations	7
§1.2.3 Superbursts	8
§1.3 Variability phenomena	9
§1.3.1 Variable emission from transient accretion	9
§1.4 The role of the crust in the model of the neutron star interior .	11
§1.4.1 Cooling of isolated neutron stars	11
§1.4.2 Superbursts in binary systems	15
2 Physics of the Crust	19
§2.1 Structure of the crust	19
§2.2 Equation of state	21
§2.2.1 Composition of the crust	22
§2.2.2 Components of the equation of state	25
§2.3 Thermal conductivity	30
§2.4 Neutrino emission	31
§2.5 Heat capacity	34

3	Simulations and Results	39
§3.1	Structure equations	39
§3.1.1	Components of the crust model	41
§3.1.2	Results and Discussion	47
§3.2	Conclusions	51

Acknowledgements

There are many people that have made my time here at McGill an enjoyable and enriching experience, both academically and personally. First of all, I wish to thank my supervisor Andrew Cumming for all his support throughout the last two years; for his advice, great patience and the opportunity to work with him.

Thanks to David Montiel for all his help and support. I am in great debt to him for his assistance to accomplish not only this project, but to all my work during this Master's Degree and his invaluable friendship. I have also received a great deal of help and wise advice from Diana Dragomir. The conversations with her and the eternal summer student Michael Zamfir brought additional amusement during the time in the office. Furthermore, I thank the support and friendship of Mary Bautista over this last year, it has been quite a nice surprise to find someone who comes from the same village, almost.

I also thank the endless support of my mother, Angeles. Wherever I am she keeps encouraging me to achieve my goals.

Finally, I thank Marie-Luise Ermisch for reading this work, make suggestions and spelling corrections.

I wish to thank the funding from the Department of Physics and the partial financial support awarded from *Secretaría de Educación Pública* from Mexico under the program *Becas Complementarias-DGRI*

Abstract

The advent of X-ray astronomy has turned the study of compact objects into one of the most active research fields in modern-day physics. Diverse luminosity phenomena have been remarked upon in neutron stars and it is believed that in many of them the neutron star crust plays a critical role. This work presents a steady-state model for the neutron star crust that describes, in particular, the profiles of temperature and flux along this region. It is divided as follows: First, a review of observational phenomena in neutron stars, where crust characteristics are thought to be crucial, are presented, alongside general aspects of the theoretical models applied. Second, the different elements that are needed to construct this model are considered. Third, the set of structure equations to be resolved and the calculations of the components of these equations are provided. Finally, the results are shown and discussed and the conclusion is presented.

Abrégé

L'avènement de l'astronomie des rayons X a transformé l'étude des objets compacts en un des champs de recherche des plus actifs en physique moderne. Divers phénomènes de luminosité ont été observés dans les étoiles neutron et on estime que la croûte de l'étoile neutron joue un rôle important dans beaucoup de ces phénomènes. Cet ouvrage présente un modèle d'équilibre stable pour la croûte de l'étoile neutron qui décrit, en particulier, les profils de température et flux dans cette région. L'ouvrage est divisé comme suit: Premièrement, une révision des phénomènes observés dans les étoiles neutron, où les caractéristiques de la croûte sont supposées être cruciaux, est présentée, avec les aspects généraux des modèles théoriques utilisés. Deuxièmement, les différents éléments nécessaires pour construire ce modèle sont examinés. Troisièmement, l'ensemble des équations de structure à résoudre et les calculs des composantes de ces équations sont présentés. Finalement, les résultats sont montrés et discutés et la conclusion est présentée.

Chapter 1

Luminosity phenomena in neutron stars

Different high luminosity events are observed in neutron stars. Although the main source of power of these events is either the core of the star or the accretion process, the crust plays an important role in regulating the release of energy and duration not only during high energy events, but also within the quiescent periods. We present a brief review of these phenomena as introduction and with the aim of illustrating the importance of the crust model in studying different types of luminosity phenomena in neutron stars.

We can classify the observed phenomena in two parts: for isolated neutron stars we consider the *cooling* of the star, whereas for binary systems we consider the events related to *accretion*. We also present a brief review of the variability phenomena observed in isolated and accreting neutron stars.

§1.1 Cooling of isolated neutron stars

Neutron stars are born as a result of a supernova explosion, with an initial temperature of $T \sim 10^{12}$ K, after which they cool down gradually. The proto-neutron star becomes transparent to neutrinos ~ 30 s after the explosion, with an equation of state almost independent of temperature in its interior (Yakovlev & Pethick, 2004). From this point the star cools by neutrino emis-

sion and heat transport. Once the heat reaches the surface of the star, it is liberated in the form of thermalized photons. This process can be analyzed considering the relativistic nature of the star (Shapiro & Teukolsky, 1983). As an example to estimate the temperature at the surface, consider a star of mass M and radius R , with T_S denoting the effective temperature. Hence, $L_\gamma = 4\pi R^2 k_B T_S^4$ is the thermal photon luminosity in the frame of reference of the star. In this way, the redshifted temperature and luminosity we can observe from the distance are

$$T_S^\infty = T_S \sqrt{1 - \frac{r_g}{R}} \quad (1.1)$$

$$L_\gamma^\infty = L_\gamma \left(1 - \frac{r_g}{R}\right),$$

where the Schwarzschild radius is defined as $r_g = 2GM/c^2 \approx 2.95 M/M_\odot$ km. Since the surface temperature can be non-uniform (v.gr. magnetized stars), a mean effective temperature of $\bar{T}_S^4 = L_\gamma/(4\pi R^2 k_B)$ is considered, where L_γ total thermal luminosity.

However, non-thermal emission is often strong enough to obscure the thermal radiation of the star. In young pulsars ($t \sim 1000$ years) this might happen due to a process in the magnetosphere, whereas in old ones ($t \gtrsim 10^6$ years) the dominant source of radiation can be located at the poles (see Yakovlev & Pethick, 2004, for a review on physical parameters of isolated neutron stars). On the other hand, isolated middle-aged neutron stars ($t \sim 10^4 - 10^6$ years) appear to be objects where the thermal emission is more noticeable within the whole spectrum. The surface temperatures for these objects ranges $T_S \sim (0.5 - 1) \times 10^6$ K, so the thermal profile is observed in soft X-rays. The detection of many features related with the cooling has been possible due to the relatively recent generation of X-ray observatories, such ROSAT (1990-1998), Chandra and XMM-Newton (both launched in 1999).

The cooling of the neutron star can be separated into three main stages (Yakovlev et al., 2008):

1. During the first 10 to 100 years, due to the much stronger neutrino emission in the core, the crust is thermally decoupled from the core.

Thus, the surface temperature is the one of the crust.

2. The star cools through high neutrino emission ($L_\nu \gg L_\gamma$) coming mainly from the core for $t \lesssim 10^5$ years.
3. For $t \gtrsim 10^5$ years the cooling is led by photons emitted from the surface ($L_\nu \ll L_\gamma$). The evolution of the internal temperature is directed by the radiation from the surface and thus is determined by the properties of the outer parts from the star.

The thermal relaxation of the star takes place during these phases. In the end, the redshifted temperature will become constant in the interior of the star, reaching a balance.

The value of T_S cannot be obtained directly, but by fitting some parameters in theoretical models applied to observational data, such as radius, surface gravity, distance and spectrum of interstellar absorption. In such models (Yakovlev & Pethick, 2004), the thermal spectrum is calculated from either a black-body spectrum or a neutron star atmosphere model which could also include a magnetic field. In models where the surface is composed of hydrogen, the depth from where the photons emerge to the surface strongly determines the hardness of the spectrum, due to the dependence of the radiative opacity on the energy of these photons. Thus, when photons come from deeper layers, their higher energy produces a harder spectrum for a given T_S than their equivalent for black-body models. Furthermore, the effective temperatures from the hydrogen atmosphere models are only half of the ones calculated using black-body models, while for an iron atmosphere both give similar T_S . Nonetheless, these atmosphere models appear to be less accurate when the stars are cooler than middle age ones ($T \sim 10^6$ K), or when a strong magnetic field requires other calculations such as ionization equilibrium or spectral opacities in magnetized plasmas.

Within the the whole model of the star (both interior and surface), the properties of the crust are fundamental to determine features such as the duration and intensity of the cooling curves. We will present a theoretical overview of the crust structure in the section §1.4 to illustrate this. Meanwhile, we

present a brief summary of different observational phenomena which motivate the construction of crust models for neutron stars.

§1.2 X-ray Burst in Binary Systems

Some variability phenomena observed in neutron stars have been attributed to the interaction of the compact star and its companion. The compact object will accrete matter from its companion over its surface (or magnetosphere), accumulating material which, under different conditions, might ignite. This leads to an increment in luminosity with respect to the one seen in quiescence.

Some parts of the crust of the neutron star are then replaced by material from the companion. What is more, the entire crust can be substituted (Brown, 2000). The density of the replaced crust, typically consisting of hydrogen and helium, is high enough ($\gtrsim 6 \times 10^{11} \text{ g cm}^{-3}$) to sustain non-equilibrium reactions that release a considerable amount of heat ($\sim 1 \text{ MeV}$ per accreted nucleon). Moreover, if the accretion is rapid enough to allow stable burning ($\dot{M} \sim 10^{-8} M_{\odot} \text{ yr}^{-1}$, typical in LMXBs), most of the heat will be conducted to the core, this results in an inversion of the thermal gradient, where the emission of neutrinos regulates the temperature.

The purity of the crust with respect to its ground state (when no accretion has taken place yet) as well as its overall composition will affect the thermal profile of the cooling of the star, which also will determine the features of the luminosity phenomena, in case unstable burning of the accreted material occurs. The latter happens when X-ray bursts take place.

§1.2.1 Overall features

The X-ray bursts were discovered in the mid-1970s, and it was just a few years later when different authors (e.g. Maraschi & Cavaliere, 1977) suggested the possibility that the X-ray bursts were due to thermonuclear flashes on the surface of accreting neutron stars. However, the discovery of the Rapid

Burster ¹ indicated that such repetitive bursts could not be explained with thermonuclear flashes, since a very high flux of persistent X-ray emission due to the release of gravitational potential energy should be present, and this was not observed.

In 1977 Hoffman² discovered that the Rapid Burster emits two different types of bursts, introducing the classification type I and type II. He claimed that the rapid and repetitive type II burst is due to accretion instabilities and the type I is due to thermonuclear flashes. Later work has strengthened the idea that this mechanism originates the bursts, although is still under debate. It was thought for some time after their discovery that bursts sources are LMXBs, and direct evidence of this has been found since the early 1980s -by means of the optical counterparts and orbital periods of the sources-. This identification has allowed the construction of models where the accretion process (through Roche lobe overflow) and the composition of accreted crust are constrained.

Neutron stars in LMXBs appear to have weak magnetic fields compared to the ones in population I binary systems. This is believed due to the absence of X-ray pulsations in LMXBs and that X-ray bursts do not occur in systems that show X-ray pulsations (Lewin et al., 1997). Therefore, it is possible to construct models of X-ray bursts where the magnetic field is less important than composition or other characteristics of the neutron star interior. Moreover, since the X-ray bursts of type I are originated in the outer layers of the neutron star, models need to include some crust composition that reflects its impurity due to accretion.

The rise and decay times are among the most important features of the bursts. The rise varies from less than a second to ~ 10 s and the decay times vary from ~ 10 s to minutes. In general the burst depends strongly on the photon energy, so when the photon energies are higher, the decay times are much shorter than at low energies. The energy dependence of the burst profile is associated with a softening of its spectrum during the decay, which seems to be a result of the cooling of the neutron star photosphere (Lewin et al., 1997).

¹A source where ~ 1000 bursts per day were observed during several weeks (Lewin et al., 1976).

²Hoffman et al. (1978)

Neutron stars in X-ray binaries increase their luminosity to $L_X \sim 10^{37}$ ergs s^{-1} during the bursts, while in the relative quiescence periods (months-decades) this luminosity is $L_X \lesssim 10^{34}$ ergs s^{-1} . The quiescence X-ray spectrum is divided into two components: a soft thermal component (black-body $kT \sim 0.2$ keV) and a power-law component that dominates the emission above 2 keV (Ushomirsky & Rutledge, 2001).

Bursts with double peak profiles have also been found. These events belong to a very energetic type I X-ray bursts during which the luminosity becomes so high (that is, it reaches the Eddington limit) that the atmosphere of the neutron star expands due to radiation pressure. Because of the rise of the radius of the photosphere, the temperature decreases and X-rays are no longer emitted. As the photospheric radius slowly starts to decrease, the temperature increases again, restarting the X-ray emission with increased energy according to the rising of the temperature. The radius stops decreasing once the surface reaches its original size, after which the photosphere cools again but without shrinking (Lewin et al., 1993).

The bursts intervals vary in regularity, on time scales of hours to days, ranging from ~ 5 minutes to days; and showing no activity in periods from days to months (although on a few regular behaviour has been observed). The bursts recurrence is sometimes related to the level of persistent X-ray emission. In some sources, like 4U 1820-303, it has been found that bursts frequency decreases when the persistent flux is increased, and the bursts stop completely if the flux increases even more. In other sources (i.e. MXB 1658-298 and GX 3+1) some burst regularity is observed while the persistent X-ray flux is relatively low (Lewin et al., 1997). Although bursts have been observed while some objects are in bright state, such as in the transient sources Cen X-4, 4U 1608-522, Aql X-1 and EXO 0748-673, the anticorrelation with respect to the bursts occurrence is maintained. However, bursts behaviour tends to be very irregular in sources with high and persistent X-ray luminosities, which could be the result of having values close to the critical that such luminosities can reach (near half of the Eddington). Above that value the bursts are not supposed to occur, according to some thermonuclear flash models. Many of the large bursts variations have been observed to be unrelated to variations in

the rate of accretion.

There are some thermonuclear models where it is implied that there is a correlation between the time interval of the bursts and their integrated energy (Lewin et al., 1997). In other words, the burst energy would be higher for longer time intervals, mainly because there would be more nuclear fuel available. The observational evidence for this hypothesis seems to point in more than one direction. Although the correlation has been observed, longer waiting times do not entail significantly larger bursts in some sources. It has also been observed that for longer time intervals between bursts, photospheric radius expansion is $\sim 10^1 - 10^2$ km, which is followed by a gradual recontraction. These radius expansion bursts are believed to be originated when the critical Eddington luminosity is exceeded and the atmospheric layers are lifted.

It is also important to mention that the luminosity observed during the quiescence ($10^{32} - 10^{33}$ ergs s^{-1} , called basal luminosity) of burst sources shows peculiarities that imply that its origin lies in the neutron star crust. According to Ushomirsky & Rutledge (2001), it has been suggested that such luminosity is caused by one of the following phenomena: a) the continued accretion in quiescence, possibly through an advection-dominated accretion flow; b) accretion onto the magnetosphere of the neutron star; and c) thermal emission from a hot core of the star heated by non-equilibrium reactions in the neutron star crust. It is considered that from all these possibilities, only the heated-thermal emission predicts the luminosities observed in the thermal spectral component, although a combination of the three is not ruled out. We will refer to the heating scenario in the description of our model.

§1.2.2 Optical Observations

There have been different campaigns of coordinated optical and X-ray observations of burst sources. The first optical/X-ray burst was detected in the object 4U 1735-444 (Grindlay et al., 1978). The fluence in the optical burst was equivalent to $\sim 2 \times 10^{-5}$ times the one observed in X-ray burst, which is ~ 6 times greater the one expected if the optical emission corresponds to the low-energy tail of the black-body X-ray burst. This and other observations

may indicate that the optical emission comes from the interaction of the X-rays of the source with the surroundings of the neutron star, i.e. the accretion disk and the companion star. The optical signal will therefore be delayed according to the distances from the source to the observer and to the place where X-rays are reprocessed and transformed into optical photons before reaching the observer. In this scheme, X-rays will illuminate the environment of the neutron star, providing information of the surrounding area in the form of optical radiation.

§1.2.3 Superbursts

In recent years a phenomenon has been discovered that is similar to the type I X-ray bursts, but notably more energetic. This phenomena is observed in about 10% of the burst sources and displays around 1000 times more energy than the regular type I X-ray burst (hence they are referred to as *superbursts*), over time scales of hours to a day (Keek et al., 2008).

So far, the superbursts have only been seen in systems where continuous accretion has been registered for at least 10 years and in sources with persistent pre-burst luminosities ($L \simeq 0.1 - 0.25L_{Edd}$). Also, when the neutron star was monitored with sufficient time in advance, a precursor burst was observed. The recurrence time of these events has not yet been well specified, although estimations are of the order of one year (Cumming et al., 2006). Around 10 superburst have been registered so far (Keek et al., 2006). Wijnands (2001) even reported two events from 4U 1636-536 which were $\simeq 4.7$ years apart. During the rise and decay of superbursts luminosity it is possible to observe how the spectrum hardens and softens, respectively. We can also see this in the spectral fits of the time-resolved pre-burst subtracted X-ray spectra, obtained during the superburst (Kuulkers, 2004).

The similarity of these events with the type I X-ray burst led to the idea that their origin lies in thermonuclear runaway events as well (although deviations from the exponential decay profile exist). However, the differences in energy and duration indicate that if the scenario of thermonuclear flashes is true, the burning layer should be much further down in the neutron star than

those where the regular bursts occur to account for the duration (Keek et al., 2008).

It is very likely that superbursts restrain the apparition of “regular” type I X-ray burst. During continuous monitoring of the source 4U 1735-444, no normal X-ray burst activity was detected after 7.5 days after the superburst, despite the X-ray flux being similar to the one observed when the objects showed normal X-ray bursts. This was also true for the sources KS 1731-260 and Ser X-1. These objects showed normal X-ray burst activity before superbursts were seen, after which no normal events were registered for around a month (Kuulkers, 2004).

Whereas the models of type I X-ray bursts rely on the unstable burning of H and/or He, it is thought that superbursts are originated from the burning of those materials but from deeper layers. Alternatively, the ignited material can include carbon, as pointed in models by Cumming et al. (2006). Different simulations using these models indicate that the superburst events are very sensitive to the thermal properties of the neutron star interior, such as accreted composition of the crust and neutrino emission (both from the core and crust). This offers the opportunity to use this kind of events to explore the interior of neutron stars, in particular the crust structure. We will see more about this in §1.4.2.

§1.3 Variability phenomena

§1.3.1 Variable emission from transient accretion

Variability of the luminosity of neutron stars during quiescence has also been observed, and it seems to represent another phenomena where the crust plays an important role. The basal luminosity during the quiescence periods of neutron stars ($10^{32} - 10^{33}$ ergs s^{-1}) is reported to vary by a factor of as much as ~ 3 or more during time-scales of days to years. There are three main scenarios considered in the literature to explain the origin of this type of variability (Ushomirsky & Rutledge, 2001):

1. Variable accretion on the neutron star. If accretion on the surface dom-

inates the luminosity in quiescence, changes in the accretion rate can be responsible for variations in the thermal part of the spectrum, since the photospheric spectrum at the assumed low accretion rate gives the required thermal emission, supposing absence of shock and an appropriate quasi-continuous accretion rate.

2. Variable accretion on the magnetosphere. The power spectral tail that appears to dominate the emission above 2 keV is explained through this process. The intensity variability of that component can be a result of accretion rate variations.
3. Variable absorption column density (N_H). The outburst may be accompanied by outflows, increasing the local column density of material. This may cause the value of the absorption column density to vary which in turn accounts for the observed variation in density.

Observations of transient variability in quiescence have been made particularly on the sources Aql X-1 and Cen X-4 —see Ushomirsky & Rutledge (2001), Rutledge et al. (2002), Campana (2005)—. Initially, the observations were difficult due to the little and poor data. But recent experiments, such as Chandra, have brought to light better data in this field.

The analysis from Rutledge et al. (2002) of the Chandra data from Aql X-1 on quiescence after an outburst in 2000 found a variable flux and X-ray spectrum. They interpreted this fluctuation in terms of variations of the neutron star effective temperature, which in turn suggested low level accretion during quiescence. It is worth mentioning that these observations were the first to show clear luminosity variation and, more importantly, an increase of temperature during quiescence. On the other hand, observations made with XMM-Newton of Cen X-4 discovered rapid (> 100 s), large ($45 \pm 7\%$ rms in the $10^{-4} - 1$ Hz range) intensity variability, especially at low energies (Campana, 2005) with no appreciable periodicities (although apparition of flares in the optical is reported).

As mentioned in §1.2.1, whether steady accretion during quiescence can sustain the observed luminosities is still debated. However, it is only through variations in the effective temperature of the neutron star that variability can be

sustained for some sources (Rutledge et al., 2002). These temperature changes can account as well for features observed in the power law tail and differences in the column density. This raises the question of the existence of mechanisms of heating deep in the crust region, more likely from non-equilibrium nuclear reactions. This idea has been explored by different research groups, in combination with accretion variation, although there are not conclusive results yet.

§1.4 The role of the crust in the model of the neutron star interior

After the above summary of observations, we present a short and general description of the theoretical models that are applied to simulate the events where the crust plays a main role. We focus on the cooling of isolated neutron stars and superbursts in binaries since these are the events where the contribution of the crust is most evident. Also, these two phenomena require models where the composition of the crust varies, so the robustness of the model can also be tested.

§1.4.1 Cooling of isolated neutron stars

Just after the neutron stars are born in the supernova explosion, the interior remains opaque to neutrinos for about one minute (Yakovlev et al., 2008). Later, the star begins its phase as a regular neutron star when it becomes transparent to the neutrinos created in its interior. Both neutrino emissivity and thermal emission of photons constitute the two main ways of cooling in neutron stars. The keystone of the contemporary simulations are the structure equations defined by Thorne (1977) to calculate the thermal evolution of the star. Considering spherical symmetry, for the energy and flux we have,

$$\frac{e^{-\lambda-2\Phi}}{4\pi r^2} \frac{\partial}{\partial r} (e^{2\Phi} L_r) = -Q + Q_h - \frac{c_T}{e^\Phi} \frac{\partial T}{\partial t} \quad (1.2)$$

and

$$\frac{L_r}{4\pi\kappa r^2} = e^{-\lambda-\Phi} \frac{\partial}{\partial r}(T e^\Phi), \quad (1.3)$$

where r is the radial coordinate, Q is the neutrino emissivity, c_T is the heat capacity (per unit volume), κ is the thermal conductivity, L_r is the luminosity (understood as the heat flux transported from the interior) and Q_h is a non-specified heating contribution (such as nuclear reactions in the crust, we will see this in the next chapter). The function Φ represents the gravitational redshift and λ the gravitational distortion of radial scales, $e^{-\lambda} = \sqrt{1 - 2Gm(r)/c^2 r}$ (m being the mass within the sphere of radius r). At the surface we have $\Phi(R) = -\lambda(R)$.

To build the model of the neutron star, it should be noted that its internal structure can be regarded as temperature independent. Therefore, some models will be determined mostly by the central density and the equation of state. In the outermost layers, where it is believed the material is non-degenerate, the thermal conduction is radiative. In deeper regions, from the crust and onwards, the heat is carried by electrons, whereas in the core it is produced by electrons, neutrons and other baryons (Yakovlev & Pethick, 2004). The models of cooling are aimed to predict the curves of $T_S^\infty(t)$ and $L_S^\infty(t)$ —see §1.1— during the thermal relaxation period of the neutron star. When this phase is over, the redshifted temperature $T_i(t) = T(r, t)e^{\Phi(r)}$ becomes constant in the star interior. The equations 1.2 and 1.3 are thus replaced by the equation of global thermal balance

$$C(T_i) \frac{dT_i}{dt} = -L_\nu^\infty(T_i) + L_h^\infty - L_\gamma^\infty(T_S), \quad (1.4)$$

where

$$L_\nu^\infty(T_i) = \int dV Q(T) e^{2\Phi},$$

$$L_h^\infty = \int dV Q_h e^{2\Phi}, \quad (1.5)$$

$$C(T_i) = \int dV c_T(T).$$

The element of proper volume is $dV = 4\pi r^2 e^\lambda dr$ and C represents the heat capacity for the whole star, whereas L_ν^∞ is the total neutrino luminosity for the

observer and L_h^∞ is the heating from intermediate layers (Yakovlev & Pethick, 2004).

Besides the ones mentioned above, other physical parameters come into play when determining the cooling of neutron stars. The most important are the following:

1. The composition of the neutron star, which in turn determines the equation of state.
2. The rate of the neutrino emissivity from the interior of the neutron star.
3. The heat capacity of the interior.
4. The thermal conductivity in the crust.
5. The heating mechanisms in the intermediate layers of the star, such as non-equilibrium nuclear reactions in the crust, frictional dissipation or rotational energy.
6. The magnetic field, although in some cases it is considered negligible. When it is strong, the magnetic field may largely modify the thermal characteristics of the neutron star.

Most of these properties are calculated independently for core and crust, so it is customary that the approach to some problems assumes a fixed model of one of these two regions to be able to modify the other and, according to what is required, explore certain features. This has been done by distinct authors (e.g. Brown, 2000 or Haensel, 2001). Their models experiment extensively with diverse properties of the crust, whereas for the core the main parameter analyzed is the neutrino emissivity. We will talk in more detail of these properties in the next chapter, when we present the model of the crust.

A strong magnetic field in the neutron star can lead the evolution of the thermal profiles from the star. It is widely believed that some observational phenomena such as soft gamma-ray repeaters (SGRs)³ and anomalous X-ray

³Sources that show large bursts of gamma-rays and X-rays at irregular intervals.

pulsars (AXPs)⁴, occur due to the presence of strong magnetic fields ($B \gtrsim 10^{14}$ G) in isolated neutron stars (Kaminker et al., 2006). These special type of neutron stars, known as *magnetars*, are thought to originate such phenomena in the course of the decay of their magnetic fields, which takes place during cooling.

One of the expected results of the presence of magnetic fields in the neutron stars is the appearance of inhomogeneities in the surface temperature. Depending on the geometry of the magnetic field, “hot spots” may arise, modifying the temperature distribution (which could also be achieved by means of rotational effects) and thus altering the luminosity profiles. Therefore, it becomes crucial to bring to light the mechanisms by which the magnetic field influences the overall emission of the stars, specially the X-ray emission. In models such as the one from Geppert et al. (2005) the consequences of “normal” magnetic field strengths ($10^{12} - 10^{13}$ G, bipolar and originated in the crust) in the surface temperature distribution are analyzed.

According to Arras et al. (2004), the evolution of the magnetic field passes through a series of equilibrium states after the sporadic release of stresses in the crust and stimulations of motion in a liquid core. It is also believed that the geometry of this field has poloidal and toroidal components (purely poloidal or purely toroidal are unstable configurations for the field). In this picture, the magnetic field would evolve according to the induction equation,

$$\frac{\partial \bar{B}}{\partial t} = \nabla \times [(\bar{v} + \bar{v}_{amb} + \bar{v}_{Hall}) \times \bar{B}] + \left. \frac{\partial \bar{B}}{\partial t} \right|_{fracture}, \quad (1.6)$$

where \bar{v}_{amb} is the speed with which the magnetic field is advected by the diffusing component (electrons/protons) of the core, $\bar{v}_{Hall} = -\bar{J}/en_e$ (n_e is the electron density number) and \bar{v} is the hydrodynamic response of the core to the combined effect of this transport processes. It is also considered that the crust, if rigid, is affected by possible fractures that would cause changes in the magnetic field in short timescales.

⁴X-ray pulsars characterized by slow rotation periods and the absence (or very small) of long term variability. Both phenomena share many similarities, although the specific physical characteristics that differentiate the two classes remain unclear (Wachter et al., 2007).

The decay of the magnetic field in the crust is given by Ohmic and Hall effects, which dictates the development of currents in that region. In fact, the timescales of decay in the crust are much shorter than those in the core, thus becoming more important, in particular, for the construction of models where the accretion contributes to the evolution of the field itself. Furthermore, the Hall effect is likely to build up stresses in the crust that can be released during SGR and AXP (Cumming et al. (2006)). It is worth mentioning that the previous is applied to study the evolution of the magnetic fields of neutron stars in binary systems as well, where accreted crust composition is considered.

With the above we finish the description of the general characteristics of the cooling models. Now we will continue with an overview on the superbursts models.

§1.4.2 Superbursts in binary systems

As we have said previously, it has been suggested that superburst are originated due to heating deep in the crust structure. It is believed that the material that fuels the superburst is produced by hydrogen and helium burning through rapid proton capture process (rp-process) around the neutron drip line, which apparently explains the extended tails of these events (~ 100 s). This process allows the production of accumulating layers of heavier elements that hinder the conduction of heat, thus increasing the thermal gradient. What is more, according to some calculations, the temperature at which this material ignites agree with the observations (Cumming et al., 2006).

Other models consider the ignited material as pure carbon going through unstable burning (the initial reaction would be $^{12}\text{C} + ^{12}\text{C} \rightarrow ^{20}\text{Ne} + \alpha$) in a layer between the crust and the accreted layers. This model (Cumming & Bildsten, 2001) has been successful in reproducing different features observed in superbursts, such as energy, recurrence time, light-curves and the expected suppression of “normal” type I X-ray burst after the superburst event (Keek et al., 2006). However, the processes under which enough quantity of carbon is produced and how unstable ignition is achieved at accretion rates of $0.1 \dot{M}_{Edd}$ (inferred in superbursters) are not totally clear. Diverse theoretical

work has been done to comprehend the characteristics by which the accreted material (hydrogen and helium) burns and transforms into the superburst fuel, reproducing the observed luminosity.

In Cumming & Macbeth (2004) it is pointed out that the unstable burning of carbon takes place at densities of $\rho \sim 10^5 - 10^6 \text{ g cm}^{-3}$, producing heavy elements (mainly iron) via rp-process and residual carbon with mass fractions of $X_c \sim 0.01 - 0.1$, which can be ignited when the mass of the ashes layer reaches $\sim 10^{25} \text{ g}$. This calculation agrees with the observed superburst energies for $X_c \simeq 0.1$ and when the release of energy from the nuclear burning is 1 MeV per nucleon. It is also possible that heavy nuclei are photodesintegrated (producing elements within the iron group) when the flash occurs, enhancing the nuclear release.

In a cooling model like this, the evolution profile is calculated through the entropy equation,

$$c_P \frac{\partial T}{\partial t} = -\epsilon_\nu - \frac{1}{\rho} \frac{\partial F}{\partial r}, \quad (1.7)$$

and the flux equation

$$F = -K \frac{\partial T}{\partial r}. \quad (1.8)$$

Unlike expressions 1.2 and 1.3, the heat source is only given by the neutrino emissivity ϵ_ν , although intermediate heat sources (e.g. non-equilibrium reactions) could be considered. Again, K is the thermal conductivity and c_P the thermal conductivity. After all the considerations about the crust structure, heating from the core (outgoing flux) and integration conditions are made (which will be described in the second chapter), the thermal evolution can be computed. In the model of Cumming & Macbeth (2004) it is found that during the firsts hours of the event, $\sim 10^{42} \text{ ergs}$ are liberated from the surface. A large ammount of this energy is conducted inwards, moving the peak of temperature deeper into the crust. Consequently, the release of energy occurs on longer timescales.

Cumming et al. (2006) affirm that cooling curves predicted by this model (flux and luminosity) agree not only to observations, but also to the prediction

of the inhibition of regular X-ray bursts after the superbursts, which is argued to be a result of the stabilization in the burning process of H/He. Another important result of this work is that the early phase of the cooling depends mostly on the energy released in the flash, whereas the late phase depends for the most part on the thickness of the layer. Since in this model the fuel is supposed to burn instantly, there are no predictions on the rise of burst.

It is worth mentioning that some models that attempt to reproduce the variability in transiently accreting neutron stars rely on crust models capable of sustaining reheating mechanisms that contribute to the appearance of the outburst and to the variability itself. Haensel & Zdunik (1990b) built a model to calculate heating due to non-equilibrium nuclear processes within the outer and inner crust for a one-component plasma, assuming that the outer layers of the matter produced in the X-ray burst consisted of pure ^{56}Fe . Their assumptions also included transitions from the ground state due to electron captures, thus maximizing neutrino losses. The results showed that the deep crustal heating, produced mainly in the inner crust, was $Q \sim 1.4$ MeV per accreted nucleon. Subsequent work using improved models (Haensel & Zdunik, 2003; Gupta et al., 2007), for example, considering multicomponent plasmas, showed that electron captures in the outer crust lead mostly to excited states of the produced heavy nuclei, which heat the material when deexcite. Hence, they considered the neutrino losses in that region to be negligible, which strongly increases the outer crust heating. This result, although important, does not significantly alter the overall heating since the outer crust contributes only a small fraction of it. Simulations of the thermal relaxation of the neutron star interior under these mechanisms of heating have been done by different groups with the aim of predicting the outburst behaviour as well as the basal luminosity in accreting binary systems (e.g. Ushomirsky & Rutledge (2001)), using some models of cooling that, at least in principle, are similar to the ones described before.

As we have seen, high-energy events on neutron stars are strongly determined by the composition and general structure of the crust. In the next chapter, we will present a general picture of the physics of the crust, introducing one by one the required pieces to build a simulation of its thermal

behaviour.

Chapter 2

Physics of the Crust

In this chapter we introduce the description of the basic ingredients to build a model of the neutron star crust. To this aim, we use theoretical models for each part that have appeared in the literature and are currently employed in different astrophysical models. In consequence, the accuracy of some of them is still actively discussed.

We begin with a review of the structure of the crust and then we divide the chapter in sections to present the equation of state, thermal conductivity, neutrino emission and heat capacity.

§2.1 Structure of the crust

When a neutron star begins the process of cooling¹ we consider the object as a “regular” neutron star (typically $M \simeq 1.4 M_{\odot}$ and $R \simeq 10$ km). At this stage, we distinguish four different regions: the core, the crust, the atmosphere and the envelope. The atmosphere and envelope contain a negligible amount of mass, but each of them play an important role in shaping the observable properties of the star.

As densities increases, we find the *outer crust*, where the matter is made of nuclei and electrons. The exact density at the top of the crust is not well known, since it can vary from $\sim 10^9$ g cm⁻³ in accreting neutron stars to $\sim 10^5$

¹The cooling stage begins when the matter becomes *transparent* to neutrinos at $T \leq 10^{10}$ K.

g cm^{-3} in isolated cooling neutron stars (Cumming et al., 2004). In a fully ionized electron-plasma, like the crust interior, this border is delimited by the parameter Γ ,

$$\Gamma = \frac{(Ze)^2}{k_B T a} \quad (2.1)$$

where

$$a = \left(\frac{4}{3} \pi n_i \right)^{-1/3}, \quad (2.2)$$

k_B is the Boltzmann constant, T the temperature, Z the atomic number, a denotes the mean inter-ion distance and n_i is the ion number density. The value of Γ is useful to set regions on the crust, in particular its outer border, where a phase transition between liquid and solid occurs when $\Gamma \simeq 175$ (Potekhin & Chabrier, 2000). Thus we will consider the crust as the region where the external layers of the neutron star become solid. These parameters are valid under the assumption that the material is constituted of one ionic species at a time, such consideration is known as the one-component plasma (OCP).

At these densities, the proximity between atomic nuclei is such that one has to consider modifications to the Coulomb energy. Such densities also set the electrons in a state of strong degeneracy, thus dominating the pressure. The electron Fermi energy increases with density, which in turn induces nuclear reactions that are energetically favourable to convert electrons and protons into neutrons (and neutrinos) by means of electrons captures, so nuclei become richer in neutrons. When density reaches $\sim 10^{11} \text{ g cm}^{-3}$, the neutrons begin to drip out of the nuclei, forming a gas around them. The apparition of these free neutrons on the material define the region called the *inner crust*.

The matter in the inner crust consists of atomic nuclei, electrons and free neutrons that increase in number with the rise of density. In this range of density the nuclei stop being totally spherical, and later disappear when the density reaches $\sim 0.5\rho_0$, where $\rho_0 = 2.8 \times 10^{14} \text{ g cm}^{-3}$ is the density of the nuclear matter at saturation, so the matter turns into a mix of protons, neutrons and electrons. This condition sets the base of the crust and the top border of the core (Potekhin & Chabrier, 2000). The crust constitutes a small part

of the whole neutron star: the outer crust extends for a few hundred meters while the inner crust extends for approximately one kilometer; together they contain a total mass of the order of $0.01M_{\odot}$.

Below the inner crust resides the *core* that encloses 99% of the total mass. Similarly to the crust, we can consider a subdivision of the core. The *outer core* extends to $\sim 2 - 3\rho_0$ and consists of neutrons with an admixture of protons, electrons and possibly muons, which at this point are all strongly degenerate (Yakovlev et al., 2008). For densities up to $\sim 2\rho_0$ the composition and equation of state of the matter are reasonably well constrained by experiments and theory on nuclear physics, where the border of the outer and inner core resides.

The inner core extends down to the stellar center, where densities of $\sim 10 - 15\rho_0$ are expected (at least for massive stars) but with an uncertain composition, although it could be the same of outer core or it can occur that low mass stars do not have an inner crust at all. Hyperions may appear in addition to nucleons, as well as exotic matter: pion or kaon condensates, strange quark matter or mixed phases. From these particles, nucleons, hyperons and quarks can be in a superfluid state (we will discuss the implications of this on the neutrino emission further on). It is noteworthy that there is currently an active discussion on the possibility that some type of neutron stars are rather strange stars, constituted totally or in part of strange quark matter (Yakovlev & Pethick, 2004).

Since our investigation is focused on the crust, the features of the core will be important only in the context of its contribution to the incoming ² flux on the bottom layer of the crust. Now we will concentrate in the characteristics of the crust in order to obtain an equation of state.

§2.2 Equation of state

We will work under the assumption of two different states for the matter in the neutron star crust. The first will be the case when the matter is in *ground state*, which corresponds to an isolated star that has gone through different nuclear reactions to produce heavier nuclei. The second will correspond to

²...or outgoing, although this possibility is not explored in our model.

the situation in which the neutron star belongs to an accreting binary system, thus modifying the composition of its crust from the ground state. To find out which composition corresponds to each particular case, we turn to those models that describe nuclear matter at high densities and pressures.

We will begin by presenting the models utilized to obtain the nuclear masses and particle fractions as a function of density, for both ground state and accreted crust. These values constitute the inputs of the equation of state, which will be tackled afterwards.

§2.2.1 Composition of the crust

Nowadays, most of the models are based on the classic paper of Baym, Pethick & Sutherland (1971)³. This model assumes that matter is in its ground state in complete thermodynamic equilibrium (cold catalized matter) and it forms a perfect crystal lattice of a single species of atomic nucleus (A, Z). Different modifications of this model has been considered over the years, as for example, the model from Haensel & Pichon (1994) which describes the matter below the neutron drip point. According to it, at a given pressure P the equilibrium value of A, Z is determined by the condition of minimum Gibbs energy per nucleon, where the lattice is modeled considering the Wigner-Seitz cell approximation. The energy of each cell is given by the expression

$$E_{cell}(A, Z) = W_N(A, Z) + W_L(Z, n_N) + \frac{[\epsilon_e(n_e, Z) + P]}{n_N}, \quad (2.3)$$

where W_N is the energy of the nucleus (including rest energy), W_L is the body-centered cubic lattice energy per cell, ϵ_e is the mean electron energy density and n_N, n_e refer to nuclei and electron number densities, respectively ($n_e = Zn_N$). The pressure for this model is calculated as

$$P = P_e(n_e, Z) + P_L(n_N, Z). \quad (2.4)$$

When at the pressure P_i the optimal values A, Z change into A', Z' , a jump in the baryon density occurs (Δn_b). This is given by the approximation

³Often referred to as BPS in the current literature

formula

$$\frac{\Delta n_b}{n_b} \simeq \frac{Z}{A} \frac{A'}{Z'} - 1, \quad (2.5)$$

which comes from the condition of continuity of pressure (we will see later that $P \simeq P_e$). In this model, the nuclear masses (and some isotopes) are taken from both experimental data and theoretical models (see Haensel & Pichon (1994) and references therein). We use the values on their table to define the crust from its base up to $\rho = 2.67 \times 10^{11}$.

After the drip point, we use the nuclear data from Douchin & Haensel (2001). In this paper, the equation of state for matter in the crust below the drip point and the core is analyzed. When no experimental data is available, there are roughly three ways to calculate parameters such as structure, composition and equation of state in the inner crust, each one corresponding to different approximations to solve the many-body problem. The first is a full quantum mechanical treatment using a Hartree-Fock approximation with an effective nucleon-nucleon interaction; the second is to approximate the many-body wave function using semi-classical Extended Thomas-Fermi approximations. The last technique is based on the Compressible Liquid Drop Model (CLDM) from the classical paper from Mackie & Baym (1977).

Although all three methods have been used in the last decades, the CLDM is widely used in contemporary literature for diverse reasons. One of them is that it enables the separation of the different contributions to the total energy of the W-S cell, so their role and mutual interaction can be identified. This is,

$$E_{cell} = E_{N,bulk} + E_{N,surf} + E_{Coul} + E_e, \quad (2.6)$$

where $E_{N,bulk}$ corresponds to the bulk contribution of nucleons, $E_{N,surf}$ gives the contribution of the interface between neutron gas and nuclear matter, E_{Coul} is the term that includes the Coulomb interactions while E_e gives the contribution of the electrons, that conform a Fermi gas.

This model has been improved by different authors. Most recently Douchin & Haensel (2001) used a particular method called Skyrme Lyon (SLy) to account for the effective nuclear interactions. The nuclear data for densities just before the drip point is taken from that paper.

Therefore, in our calculations we use data from Douchin & Haensel (2001) to obtain the parameters from the bottom layers of the outer crust, so we omit the use of values for a couple of density layers —just before the drip point— from the tabulation in Haensel & Pichon (1994). Here we follow the same convention found in Cumming et al. (2004).

In the case of the composition of accreted crust, we turn to the work of Haensel & Zdunik (1990a). They suggest an extrapolation of the CLDM model for the case of rich nuclei immersed in a neutron gas, when no experimental data is available. The presence of this gas would exert pressure on the nuclei, thus decreasing the surface nuclear energy. Similarly to eq. 2.3, the Gibbs energy of the cell can be written as

$$E_{cell}(A, Z) = W_N(A, Z, n_n) + W_L(n_N, Z) + \frac{[\epsilon_e(n_e) + (1 - n_N V_N)\epsilon_n(n_n) + P]}{n_N}, \quad (2.7)$$

where V_N represents the volume of the nucleus and n_n the number density of neutrons that form the gas. The pressure in this model is calculated as

$$P = P_e(n_e, Z) + P_L(n_N, Z) + P_n(n_n). \quad (2.8)$$

At a given pressure, the equilibrium value of Z is determined by minimizing the Gibbs energy of the unit cell. The calculation of the density profile of an accreted crust show that, in order to compress an initial density of $\sim 10^8$ g cm $^{-3}$ to the density $\sim 6 \times 10^{11}$ g cm $^{-3}$ (where the drip point is believed to be in this case), the star has to accrete a mass of $3 \times 10^5 / \dot{M}_{-10}$ years, where \dot{M}_{-10} is the accretion rate in units of $10^{-10} M_\odot$ /year. Compression up to the maximum density considered in the model (1.2×10^{13} g cm $^{-3}$) would require accretion of $\sim 5 \times 10^{-4} M_\odot$, that in turn needs $\sim 5 \times 10^6 / \dot{M}_{-10}$. After this time the entire crust up to the considered densities would consist of non-catalyzed matter (Haensel, 2001).

To obtain the composition, the evolution of an element of matter produced from the helium burning under the compression due to accretion is considered. Below this layer, the material ($A = 56$, $Z = 26$) should go through the reaction

${}^{56}\text{Fe} + e^- \rightarrow {}^{56}\text{Mn} + \nu_e$. In general, the nucleus enriches approximately under the scheme

$$\begin{aligned} (A, Z) + e^- &\rightarrow (A, Z - 1) + \nu_e \\ (A, Z - 1) + e^- &\rightarrow (A, Z - 2) + \nu_e. \end{aligned} \tag{2.9}$$

The neutron drip begins with reactions of neutron capture, which gives place to a chain of non-equilibrium reactions. The process follows ${}^{56}\text{Ar} \rightarrow {}^{52}\text{S} + 4n - 2e^- + 2\nu_e$. The electron captures cause the values of Z to decrease as the density rises, until the point where fusions of nuclei take place, through pycnonuclear reactions. That begins with ${}^{34}\text{Ne} + {}^{34}\text{Ne} \rightarrow {}^{68}\text{Ca}$, therefore reducing the number of nuclei by one half when the processes are completed. These reactions might constitute an important source of heat in the crust, as we will see when we discuss the neutrino emission (Haensel, 2001).

The composition of both inner and outer crusts for an accreting neutron star is taken from a table in Haensel & Zdunik (1990b). As we can see, the nuclear masses vary with respect to the matter in ground state. For example, above the neutron drip, the atomic number Z for accreting stars remains lower than the one for catalyzed matter, as well as the values for mass number A . It is worth noting that the value of the neutron drip does not greatly vary in either situation: for isolated and accreted compositions $\rho_{drip} \simeq 10^{11} \text{ g cm}^{-3}$.

It is also notable that the composition values for isolated crust after the neutron drip have been extrapolated, according to the results of the papers used to obtain the data (non-integer values for Z and A , Haensel & Pichon (1994) and Douchin & Haensel (2001)).

§2.2.2 Components of the equation of state

Electrons, nucleons and free neutrons each contribute to the pressure in the crust. Thereby we divide the calculation of the equation of state into these three parts.

Electrons

In the whole crust the pressure is high enough to compel the electrons to be in a state of degeneracy, thus forming a Fermi gas. Hence the equation of state

depends only on density and composition.

Let us consider an ideal gas of fermions, with arbitrary relativity ($v \ll c$ or $v \sim c$). The number of states with energy E is given by the expression

$$g(E) = \frac{8\pi p^2}{h^3 v}. \quad (2.10)$$

On the other hand, for a Fermi gas, the occupation number of a state with energy E is

$$f(E) = \frac{1}{1 + e^{(E-E_F)/k_B T}}, \quad (2.11)$$

where E_F is the Fermi energy. Therefore, the number density of particles with energy between E and dE is

$$n = \int f(E)g(E)dE, \quad (2.12)$$

with an internal energy given by

$$U = \int f(E)g(E)dE. \quad (2.13)$$

To obtain the pressure we multiply eq. 2.12 by the moment flux across a unit area (and passing within a solid angle $d\Omega$) given by $\int d(\cos \theta)p(\cos \theta)(v \cos \theta)$. Thus pressure becomes

$$P = \frac{1}{3} \int p v f(E)g(E)dE. \quad (2.14)$$

Since we consider the case where electrons form a completely degenerate gas, $E_F \gg k_B T$ holds. Thus for eq. 2.11 we get

$$f(E) = \begin{cases} 1 & \text{if } E < E_F \\ 0 & \text{if } E > E_F. \end{cases} \quad (2.15)$$

Integrating eq. 2.12 over momentum we obtain

$$n = \int^{p_F} \frac{8\pi p^2 dp}{h^3} = \frac{1}{3\pi^2} \left(\frac{p_F}{\hbar} \right)^3 \quad (2.16)$$

where $p_F = \hbar k_F$ is the Fermi momentum. We define the Fermi wave vector as

$$k_F = (3\pi^2 n)^{1/3}. \quad (2.17)$$

In the relativistic and non-relativistic limits, we have for the Fermi energy

$$E_F = p_F c \propto n^{1/3} \quad \text{relativistic.} \quad (2.18)$$

and

$$E_F = \frac{p_F^2}{2m} \propto n^{2/3} \quad \text{non-relativistic.} \quad (2.19)$$

Finally, using the above relations, the pressure in those limits gives

$$P = \frac{1}{4} n E_F \quad \text{relativistic.} \quad (2.20)$$

and

$$P = \frac{2}{5} n E_F \quad \text{non-relativistic.} \quad (2.21)$$

To find the relations between particles abundances in degenerate gases, it is customary to work with units of number (Y_j) and mass (X_j) fraction, where the index refers to the particle species. The expressions

$$\rho Y_j = n_j m_p \quad (2.22)$$

$$\rho X_j = (A_j m_p) n_j,$$

define such number and mass fractions, respectively. However, since our model contemplates only one atomic species at a time, then $A_j = 1$ and thus $Y_j = X_j$. We keep the notation Y_j to indicate number fractions, except for neutrons, where it is customary to use the notation X_n .

First we get the relations between nuclei (i) and neutrons (n) using $\rho = A m_p n_i + m_p n_n$ and eq. 2.22,

$$1 = A Y_i + Y_n. \quad (2.23)$$

On the other hand, since $n_e = Z n_i$, we have $Y_e = Z Y_i$. Combining this with

eq. 2.22 we obtain

$$Y_e = \frac{Z}{A}(1 - Y_n). \quad (2.24)$$

These relations are very useful to simplify the expressions for the electron pressure. In the relativistic case, we do this by replacing values in eq. 2.20 from relations 2.18, 2.17 for the Fermi momentum, and 2.22 to obtain an expression in terms of the electron number fraction. Once we replace the constant values we get

$$P_e = 1.23244 \times 10^{15} Y_e^{4/3} \rho^{4/3} \text{ erg cm}^{-3}. \quad (2.25)$$

In the inner and outer regions of the crust the electrons are relativistic (Cumming et al., 2004), so their contribution to the total pressure will be calculated only using the previous equation.

Neutrons

The neutrons that drip from nuclei are non-relativistic. According to the CLDM from Mackie & Baym, the neutron chemical potential for pure neutron matter μ_n can be calculated by means of the expression

$$\mu_n = W(k, 0) + \frac{1}{3}k \frac{\partial W(k, 0)}{\partial k} \quad (2.26)$$

where $W(k, 0)$ is a term that contains the bulk energy per baryon, and accounts for the neutron-neutron interactions (the energy units are MeV). This can be approximated by the equation

$$W(k, 0) = c_0 k + c_1 k^2 + c_2 k^3 + c_3 k^4 \quad (2.27)$$

where

$$c_0 = 1.2974, \quad c_1 = 15.0298, \quad c_2 = -15.2343, \quad c_3 = 7.4663.$$

Therefore, eq. 2.26 becomes

$$\mu_n = \frac{4}{3}c_0 k + \frac{5}{3}c_1 k^2 + 2c_2 k^3 + \frac{7}{3}c_3 k^4. \quad (2.28)$$

In these equations, $k = (3/2 \pi^2 n_n)^{1/3}$ as appears in the original paper from Mackie & Baym, which is slightly different to the definition of Fermi wave vector in eq. 2.17. Due the strong degeneracy, $\mu_n = E_{F,n}$ holds and we can simply replace the above calculation in the expression 2.21 to obtain the neutron pressure

$$P_n = \frac{2}{5} \mu_n n_n \quad (2.29)$$

Nuclei

The overall pressure is dominated by electrons and neutrons throughout the crust as will be shown further on. Due to this, we only considered a oversimplified calculation of the ion contribution.

Let us consider an ideal gas of ions. Thus pressure is given by

$$P_n = n_i k_B T \quad (2.30)$$

where n_i corresponds to the mass fraction of ions, which can be obtained using $Y_e = ZY_i$ in equation 2.24.

Total pressure

For the total pressure, we consider only the contributions of electrons, neutrons and ions. Therefore

$$P_{tot}(\rho, T) = P_e + P_n + P_i. \quad (2.31)$$

To obtain the pressure, we use the nuclear data from the tables mentioned in the section §2.2.1, assuming that the calculations shown hold for both ground state and accreted crust, so the composition and density are enough to obtain a good approximation of the pressure value in each case. The model is largely simplified if we do not include the contributions of the Coulomb energies to the pressure, as in fact, they are not relevant to the calculation of the overall pressure.

§2.3 Thermal conductivity

To obtain an expression for the thermal conductivity in the crust is crucial for the calculations that allow the prediction of the features of the luminosity observed in the star. The conducted flux is originated largely in the core and conducted through the crust on its way to the surface. For a material in degenerate state, the heat conduction is dominated by electrons.

According to Schatz et al. (1999), The conductivity can be written as

$$\begin{aligned} K &= \frac{\pi^2 k_B^2 T n_e}{3m_* \nu_c} \\ &= 4.1 \times 10^{17} \text{erg cm}^{-1} \text{s}^{-1} \text{K}^{-1} \rho_6 T_8 \left(\frac{10^{16} \text{s}^{-1}}{\nu_c} \right) \frac{Y_e}{(1+x^2)^{1/2}}, \end{aligned} \quad (2.32)$$

where the collision frequency $\nu_c = \nu_{ei} + \nu_{ee}$ includes the contribution of electron-ion and electron-electron collisions, respectively; $m_e^* = m_e + E_F/c^2$ (E_F the Fermi energy including the rest mass) and x is the relativistic factor calculated as $x = p_F/(m_e c)$.

The electron-ion collision frequency ν_{ei} is given by

$$\nu_{ei} = \frac{4e^2 m_*}{3\pi \hbar^3} \frac{\sum_i Y_i Z_i^2}{Y_e} \Lambda_{ei} = 1.8 \times 10^{16} \text{s}^{-1} \frac{\sum_i Y_i Z_i^2}{Y_e} \Lambda_{ei} \left(\frac{m_e^*}{m_e} \right), \quad (2.33)$$

where the Coulomb logarithm Λ_{ei} is calculated as

$$\Lambda_{ei} = \Lambda_{ei}^0 - \frac{v_F^2}{2c^2}; \quad \Lambda_{ei}^0 = \ln \left(\frac{r_{max}}{r_{min}} \right) \quad (2.34)$$

and $v_F = p_F/m_e^*$. Λ_{ei}^0 represents a relativistic correction to the cross-section while r_{max} and r_{min} are the limits of the integral over impact parameters. This parameter can be rewritten if we observed that Γ of the mixture is

$$\Gamma = \frac{e^2}{k_B T a} \frac{\sum_i n_i Z_i^2}{\sum_i n_i} = 0.23 \left(\frac{\sum_i Y_i Z_i^2}{\sum_i Y_i} \right) \frac{(\rho_6 \sum_i Y_i)^{1/3}}{T_8}, \quad (2.35)$$

so Λ_{ei}^0 from eq. 2.34 becomes

$$\Lambda_{ei}^0 = \ln \left[\left(\frac{2\pi\pi}{3} \right)^{1/3} \left(\frac{Ye}{\Sigma_i Y_i} \right)^{1/3} \left(\frac{3}{\Gamma} + \frac{3}{2} \right)^{1/2} \right], \quad (2.36)$$

and thus, combined with eq. 2.34 and eq. 2.35 gives the value of ν_{ei} .

On the other hand, to obtain the electron-electron collision rate ν_{ee} we use the fitting formula from Potekhin et al. (1997):

$$\nu_{ee} = \frac{3\alpha^2(k_B T)^2}{2\pi^3 \hbar m_e^* c^2 b_e^{3/2}} J(y), \quad (2.37)$$

where $y = \sqrt{3}T_{pe}/T$, which in turn includes the quantities

$$T_{pe} = \frac{\hbar\omega_{pe}}{k_B}, \quad \omega_{pe} = \sqrt{\frac{4\pi e^2 n_e}{m_e^*}}, \quad (2.38)$$

that represent the electron plasma temperature and frequency, respectively. Also, $\alpha = e^2/(\hbar c)$, $\beta = x/\sqrt{1+x^2}$ and $b_e = \alpha/(\pi\beta)$. Lastly, $J(y)$ is approximated by another fitting (for different relativistic values x and y) by

$$J = \left(1 + \frac{1}{5x^2} + \frac{2}{5x^4} \right) \left[\frac{y^3}{3(1+0.07414y)^3} \ln \left(\frac{2.810 - 0.810\beta^2 + y}{y} \right) + \frac{\pi^5}{6} \frac{y^4}{(13.91 + y)^4} \right] \quad (2.39)$$

that reproduces the exact solution for the ν_{ee} within 3.7% of mean error, according to the authors.

The above allows us to calculate the overall collision rate ν_c that we need in order to determine the thermal conductivity. We will see how this incorporates the overall thermal behaviour of the crust in the next chapter.

§2.4 Neutrino emission

The calculation of the neutrino emission is separated into two parts, one for neutrinos produced at the core and one for those created at the crust. The

characteristics from the neutrino emission in the core are particularly important, as they determine what is the amount of thermal energy available at the base of the crust (incoming flux) that can be conducted throughout it (in the way seen in the last section §2.3). On the other hand, the rate of neutrino emission in the crust will let us know what amount of that thermal energy is actually conducted to the surface and how much is lost in form of neutrinos.

Neutrinos from the core

In a core formed by non-superfluid matter, the mechanisms of production of neutrinos are divided into slow and fast ones. The emissivity Q_ν for each of this processes is calculated as

$$Q_{slow} = Q_s T_9^8, \quad Q_{fast} = Q_f T_9^6. \quad (2.40)$$

The values of the factors Q_f and Q_s depend on the type of nuclear reaction occurring in the core. For the slow neutrino emission we have *Bremsstrahlung*,



that liberates $Q_s \simeq 10^{20} - 3 \times 10^{21}$ [erg cm⁻³ s⁻¹], and *Modified Urca*,



that produces $Q_s \simeq 10^{20} - 3 \times 10^{21}$ [erg cm⁻³ s⁻¹] (Yakovlev et al., 2008). The most powerful emission comes from a direct Urca process in nucleon or nucleon/hyperon matter, which corresponds to the emission of a pair neutrino-antineutrino by means of beta decay and neutron and electron capture on a proton ($Q_s \simeq 10^{26} - 3 \times 10^{27}$). A modified Urca by an additional neutron N required by conservation of energy and momentum, these mechanisms are classified in nn, np and pp for dense npe matter.

According to eq. 2.40, the neutrino luminosities can vary largely for different stars. This is due to the differences in the inner core densities for massive or low-mass stars (where the inner core can be even suppressed). In a young

massive star, for example, neutrinos are emitted by direct Urca in a core at $T = 10^9$ K, so the luminosity L_ν reaches $\sim 10^{46}$ erg s $^{-1}$, while in a low-mass star at the same temperature, the luminosity can be ~ 7 orders of magnitude lower. In both cases L_ν decreases appreciably with time, for instance, in a low-mass star $L_\nu \sim 10^{34}$ erg s $^{-1}$ after $\sim 10^6$ years (Yakovlev et al., 2008).

In the case of superfluid cores, the neutrino emission is largely diminished. This occurs when the temperature T drops below the critical temperature T_c of a given baryon species, producing an energy gap in the baryon energy spectrum that suppresses all the reactions where they participated (Yakovlev & Pethick, 2004). We do not consider this case in our model, so the energy available at the base of the crust (incoming flux) is assumed as originated by non-superfluid cores.

Neutrino emission in the crust

Part of the non-neutrino flux coming into the base of the crust is lost in form of neutrinos, influencing the luminosity profiles of the neutron star. Throughout the crust, the neutrino pair bremsstrahlung is assumed to be the major mechanism of neutrino losses. This process is written, in general, as

$$e + (Z, A) \rightarrow e + (Z, A) + \nu + \bar{\nu}. \quad (2.43)$$

which takes place under either neutral or charged electroweak currents. According to Kaminker et al. (1999), this process is valid only when $T \lesssim 5 \times 10^9$ K, up to where the nuclei are not dissociated. Our calculations for the rate of neutrino loss are based on the paper of this authors.

The emission mechanisms for neutrinos are different for crusts in liquid or solid states (sec. §2.1). In the liquid phase the neutrinos come from the scattering of electrons by nuclei while in the solid state they come from two processes: electron-phonon scattering (known as the phonon contribution) and the Bragg diffraction of electrons (static-lattice contribution).

The general expression for the neutrino emissivity from neutrino-pair bremsstrahlung for relativistic degenerate electrons in a plasma of spherical

nuclei is written as

$$Q = \frac{8\pi G_F^2 Z^2 e^4 C_+^2}{567\hbar^9 c^8} (k_B T)^6 n_i L \quad (2.44)$$

$$\simeq 3.229 \times 10^{11} \rho_{12} Z Y_e T_8^6 L \quad \text{erg s}^{-3},$$

where $G_F = 1.436 \times 10^{-49}$ represents the Fermi weak coupling; the factor $C_+ = C_V^2 + C_a^2 + 2(C_V'^2 + C_a'^2)$ represents the constants for the weak interaction: the first two for electron neutrinos, while the other two correspond to muonic and tauonic neutrinos. The parameter L includes the mentioned contributions for different phase states. In liquid $L = L_{liq}$ while in solid $L = L_{ph} + L_{sl}$ (phonon and static-lattice contributions). The calculations of each of this contributions can be approximated by the fitting formula:

$$\log Q = 11.204 + 7.304\tau + 0.2976r - 0.370\tau^2 + 0.188\tau r - 0.103r^2 \quad (2.45)$$

$$+ 0.0547\tau^2 r - 6.77 \log(1 + 0.220\rho/\rho_0),$$

where $\tau = \log T_8$, $r = \log \rho_{12}$ and $\rho_0 = 2.8 \times 10^{14} \text{ g cm}^{-3}$. This formula gives the emissivity Q (units in erg cm^{-3}) for the ranges $10^9 \text{ g cm}^{-3} \leq \rho \leq 1.5 \times 10^{14} \text{ g cm}^{-3}$ and $5 \times 10^7 \text{ K} \leq T \leq 2 \times 10^9 \text{ K}$, where the nuclei is expected to be spherical (except maybe within $10^{14} \text{ g cm}^{-3} \leq \rho \leq 1.4 \times 10^{14} \text{ g cm}^{-3}$) with a relative error of 1% with respect to the exact solutions. To the purposes of our model, the above fitting gives an appropriate rate to calculate the neutrino losses.

§2.5 Heat capacity

We saw in the first chapter how the thermal evolution of the star depends on the heat capacity for cooling models (e.g. eq. 1.2). The main contributors to the heat capacity in the crust are the ions. We will consider only heat capacity for ions and for electrons. We will again show calculations for each contribution separately.

Ions

The calculation is separated into two parts; the liquid and solid crust. As we have seen in section §2.1, the regions are defined by the value of the coupling parameter Γ (eq. 2.1). Hence, a phase transition occurs when $\Gamma \simeq 175$.

In the liquid “ocean” ($\Gamma < 175$), we will use the heat capacity approximation calculated by Potekhin & Chabrier (2000). Their model calculates the Helmholtz free energy of electron-ion plasmas (one-component plasma), consisting in different species of point-like ions and electrons for a wide range of degeneracy and relativity. According to the model, considering that all the thermodynamic functions of the “classical” OCP can be expressed as functions of the only parameter Γ , the expansion of the internal energy yields

$$\begin{aligned}
 u_{ii} \equiv \frac{U_{ii}}{N_i k_B T} = & -\frac{\sqrt{3}}{2} \Gamma^{3/2} - 3\Gamma^3 \left[\frac{3}{8} \ln(3\Gamma) + \frac{C_E}{2} - \frac{1}{3} \right] \\
 & - \Gamma^{9/2} (1.6875\sqrt{3} \ln \Gamma - 0.23511) + \dots
 \end{aligned}
 \tag{2.46}$$

The first term corresponds to the Debye-Hückel energy, the second comes from the model of energy expansion of Abe (1959) —where $C_E = 0.57721$, the Euler constant—, while the third one from the model of Cohen & Murphy (1969). In this manner, the free energy is obtained by integration:

$$\begin{aligned}
 f_{ii} \equiv \frac{F_{ii}}{N_i k_B T} = & \int_0^\Gamma \frac{u_{ii}(\Gamma')}{\Gamma'} d\Gamma' = -\frac{\Gamma^{3/2}}{\sqrt{3}} - \Gamma^3 \left(\frac{3}{8} \ln \Gamma + 0.24225 \right) \\
 & - \Gamma^{9/2} (0.64952 \ln \Gamma - 0.19658).
 \end{aligned}
 \tag{2.47}$$

Even so, the above expression does not apply for $\Gamma \gtrsim 1$. For the range $1 \leq \Gamma \leq 200$, Potekhin & Chabrier use results from Dewitt & Slattery (1999), who obtained data from Monte Carlo simulations, as well as the corresponding analytic fits. But since these fits does not reproduce data at small Γ , Potekhin

& Chabrier propose their own parametrization:

$$u_{ii} = \Gamma^{3/2} \left[\frac{A_1}{\sqrt{\Gamma + A_2}} + \frac{A_3}{\Gamma + 1} \right] + \frac{B_1 \Gamma^2}{\Gamma + B_2} + \frac{B_3 \Gamma^2}{\Gamma^2 + B_4}, \quad (2.48)$$

where $A_3 = -\sqrt{3}/2 - A_1/\sqrt{A_2}$. This expression is an improved version of a model proposed by the same authors in a previous paper (Chabrier & Potekhin, 1998), where only the terms in the square brackets were considered. In the above expression, the term with B_1 reproduces the data from Monte Carlo simulations at large Γ , whereas the last term adjusts to eq. 2.46 at small Γ . Therefore, with eq. 2.48 in mind, the free energy is obtained from eq. 2.47:

$$\begin{aligned} f_i = & A_i \left[\sqrt{\Gamma(A_2 + \Gamma)} - A_2 \ln \left(\sqrt{\Gamma/A_2} + \sqrt{1 + \Gamma/A_2} \right) \right] \\ & + 2A_3 \left[\sqrt{\Gamma} - \arctan \sqrt{\Gamma} \right] + B_1 \left[\Gamma - B_2 \ln \left(1 + \frac{\Gamma}{B_2} \right) \right] \\ & + \frac{B_3}{2} \ln \left(1 + \frac{\Gamma^2}{B_4} \right), \end{aligned} \quad (2.49)$$

where

$$\begin{aligned} A_1 = -0.9070 \quad A_2 = 0.62954 \quad A_3 = -0.86602540 - (A_1/\sqrt{A_2}) \\ B_1 = 4.56 \times 10^{-3} \quad B_2 = 211.6 \quad B_3 = -1.0 \times 10^{-4} \quad B_4 = 4.62 \times 10^{-3} \end{aligned} \quad (2.50)$$

are fitting parameters. The heat capacity is calculated from the thermal free energy as $C_v \partial E / \partial T$; according to their calculations this gives

$$\begin{aligned} \frac{C_{v,i}}{N_i k_B} = & \frac{\Gamma^{3/2}}{2} \left[A_3 \frac{\Gamma - 1}{(\Gamma + 1)^2} - \frac{A_1 A_2}{(\Gamma + A_2)^{3/2}} \right] \\ & + \Gamma^2 \left[B_3 \frac{\Gamma^2 - B_4}{(\Gamma^2 + B_4)^2} - \frac{B_1 B_2}{(\Gamma + B_2)^2} \right], \end{aligned} \quad (2.51)$$

which represents the dimensionless heat capacity for the liquid ocean. When crystallization occurs ($\Gamma > 175$), however, there are quantum effects that have to be taken into account. In this case we turn to the model of Chabrier et al. (1992) which deals with the calculation of the free energy of a lattice. The energy of the states is calculated using an Einstein model (all modes vibrate

at the same frequency ω) for a longitudinal mode and a Debye model (linear dispersion approximation, $\omega = ck$ where c is the speed of light and k the wave vector, for the vibrational spectrum ⁴) for the transverse modes. Considering that the relation

$$E = F - T \frac{\partial F}{\partial T} \quad (2.52)$$

gives the thermal free energy per particle of the lattice, they found that

$$\frac{F}{N_i k_B T} = \frac{E_0}{N_i k_B T} + \left[-\frac{2}{3} D_3(\alpha\eta) + 2 \ln(1 - e^{-\alpha\eta}) \right], \quad (2.53)$$

where the dimensionless parameter η is given by

$$\eta = \frac{\hbar\omega_p}{k_B T} = \frac{\hbar}{k_B T} \left(\frac{4\pi Z^2 e^2 n_i}{A m_p} \right)^{1/2} = 7.76 \times 10^{-5} \frac{Z Y_i^{1/2} \rho^{1/2}}{A^{1/2} T_8}, \quad (2.54)$$

the parameters $\alpha = 0.399$, $\gamma = 0.899$ are taken from Potekhin & Chabrier (2000). D_3 corresponds to the Debye function

$$D_3(x) = \frac{3}{x^3} \int_0^x \frac{t^3 dt}{e^t - 1}, \quad (2.55)$$

and the ratio of the zero-point energy to the kinetic energy is

$$\frac{E_0}{N_i k_B T} = \frac{3}{2} \eta \mu_1, \quad (2.56)$$

where the first moment of the frequency spectrum is $\mu_1 = 0.511$. In order to calculate the free energy, it is useful to note that derivatives of the Debye function can be expressed in terms of the Debye function itself. In other words,

$$\frac{1}{3} x D_3'(x) = \frac{x}{e^x - 1} - D_3(x). \quad (2.57)$$

Therefore, utilizing eq. 2.52 we get

$$\frac{E}{N_i k_B T} = \frac{E_0}{N_i k_B T} + 2 D_3(\alpha\eta) + \frac{\gamma\eta}{e^{\gamma\eta} - 1}, \quad (2.58)$$

⁴This approximation is found in Landau & Lifshitz (1969), among others classical textbooks.

so the heat capacitance gives

$$\frac{C_{v,i}}{N_i k_B} = \frac{E - E_0}{N_i k_B T} - 2\alpha\eta D'_3(\alpha\eta) + \frac{\gamma\eta}{e^{\gamma\eta} - 1} \left[\frac{\gamma\eta e^{\gamma\eta}}{e^{\gamma\eta} - 1} - 1 \right]. \quad (2.59)$$

The previous equation can be further simplified using the eq. 2.57, so we get

$$\frac{C_{v,i}}{N_i k_B} = 8D_3(\alpha\eta) - \frac{6\alpha\eta}{e^{\alpha\eta} - 1} + \frac{\gamma^2 \eta^2 e^{\gamma\eta}}{(e^{\gamma\eta} - 1)^2}. \quad (2.60)$$

The validity of the above expression is reinforced due to its reproduction of the limit for low densities ($\eta \ll 1$), that is, it gives the expected value $C_{v,i} \rightarrow 3N_i k_B$. The evaluation of D_3 can be done by either solving the integral from eq. 2.55 or using the fitting formula (Landau & Lifshitz, 1969),

$$D_3(x) \simeq \begin{cases} f(x) = \frac{\pi^4}{5x^3} - \frac{3e^{-x}}{x^3} (6 + x(6 + x(3 + x))) & \text{if } x \gg 1 \\ g(x) = 1 - \frac{3}{8}x + \frac{1}{20}x^2 & \text{if } x \ll 1, \end{cases} \quad (2.61)$$

and using the criterion $D_3(x) \simeq \text{Min}(f(x), g(x))$. Using this expression, the value of $D_3(\alpha\eta)$ has a maximum error of 5% compared to the numerical solution of 2.55 within the range of densities and composition we use (see next chapter).

Electrons

For degenerate relativistic electrons we simply use the expression:

$$C_{v,e} = \pi^2 \left(\frac{Y_e k_B}{m_p} \right) \left(\frac{k_B T}{E_F} \right). \quad (2.62)$$

So far we have presented all the elements used in our model of the neutron star crust. In the following chapter we will show how the parts are combined when we introduce the structure equations.

Chapter 3

Simulations and Results

In this chapter we describe the model we built for the neutron star crust. We first introduce the system of equations to be solved in order to reproduce the structure of the crust and obtain the thermal and flux profiles. To this aim, we also present the individual results for the equation of state, thermal conduction, neutrino emissivity and heat capacity based on the models shown in the previous chapter. Finally, we will show our results for the model and conclusions.

§3.1 Structure equations

Our model assumes that the crust is under hydrostatic balance in steady state. Furthermore, heating produced by possible compression (e.g. caused by accretion) is ruled out, since it is of an order negligible throughout the degenerate crust and core (Brown, 2000). Hence, the internal pressure comes only from internal heating release in equilibrium against self-gravity. The hydrostatic balance is justified due to the thermal-timescale of the crust (from days to years), which is much longer than the crossing time for sound (milliseconds). Moreover, the equation of state is almost independent of temperature. Thus, the crust hydrostatic structure can be regarded as independent of the thermal evolution of the star.

Let us consider a shell of infinitesimal thickness dr at the distance r from the center of a spherical star. The mass of the shell would be given then by

$M_{r+dr} - M_r = dM_r = 4\pi r^2 \rho(r) dr$, or in the integral form $M_r = \int_0^r 4\pi r^2 \rho dr$. Now, if the local gravity given by $g(r) = GM_r/r^2$ is acting on an element of volume $1\text{cm}^2 \times dr$ in the shell, the attractive force would be

$$\rho g dr = \rho \frac{GM_r}{r^2} dr. \quad (3.1)$$

Assuming hydrostatic equilibrium, there should exist a force to counterbalance the gravitational pull, that is, the pressure. The net pressure on the shell is $P(r) - P(r + dr) = -P(dP/dr)dr$. Differentiating this expression we find the equation of motion

$$\rho \ddot{r} = \rho \frac{GM_r}{r^2} dr. \quad (3.2)$$

In hydrostatic equilibrium $\ddot{r} = 0$. So we get

$$\frac{dP}{dr} = -\frac{GM_r}{r^2} \rho = -g\rho. \quad (3.3)$$

Since the quantities g, ρ are both positive, the pressure gradient should be negative, decreasing as the radius increases. This condition represents the balance in the crust that we use as the framework for the flux and thermal transport equations. We will see this below.

Firstly, the heat is transported by conduction, so a good approximation is Fick's law of diffusion,

$$F = -K \frac{dT}{dr} \quad (3.4)$$

where the diffusion coefficient is equal to the conductivity K . Secondly, the temperature profile follows the heat equation,

$$c_p \frac{\partial T}{\partial t} = \epsilon_\nu - \frac{1}{\rho} \frac{\partial F}{\partial r} \quad (3.5)$$

in one dimension. In this equation c_p represents the heat capacitance and ϵ_ν the thermal energy lost in form of neutrinos. Since we consider only steady-state, the above becomes

$$\frac{dF}{dr} = \rho \epsilon. \quad (3.6)$$

To solve these equations we adopt a plane-parallel approximation. That is, we assume that gravity g through the thickness of the crust is constant, along with the redshift factor $1 + z$. This is certainly a good approximation due to the relatively small extension (and mass content $\sim 0.01 M_{NS}$) of the crust with respect to the whole neutron star. Furthermore, it is useful to avoid the integration of the full structure of the star since we can solve the equations in terms of a new independent variable, the column depth y . This change of variable is

$$dy = -\rho dz \quad (3.7)$$

and then, the above equations 3.4 and 3.6 become

$$\frac{dT}{dy} = \frac{F}{K\rho}, \quad \frac{dF}{dy} = \epsilon_\nu. \quad (3.8)$$

These equations represent the system to be resolved. Before we discuss the boundary conditions, we will show some results on each of the parameters presented in chapter 2.

§3.1.1 Components of the crust model

Equation of state

For the equation of state we have degenerate electrons, neutrons and ions. We follow the equations 2.25, 2.29 and 2.30 to obtain the total pressure. Each of this contributions can be seen in fig. 3.1. There we can see how the degenerate electrons dominate the pressure from the surface of the crust (set as $\rho = 10^9$ g cm⁻³) up to the neutron drip ($\rho \sim 3 \times 10^{11}$ g cm⁻³ for isolated composition and $\rho \sim 6 \times 10^{11}$ g cm⁻³). After this point the free neutrons begin to dominate the pressure. Note that the ion pressure is always much lower than that of electrons and neutrons. In these two plots, the temperature is $T = 10^8$ K and constant through the extent of the crust. Even for higher temperatures (e.g. $T \sim 10^9$) the ion pressure is kept at low values, at most $P_i \sim 10^{28}$ g cm⁻³ at the base of the crust, well below P_e and P_n .

There is a change in slope of the pressure in both situations, beyond the

neutron drip. This is due to the series of electron captures during the reactions that produce the free neutrons, thus reducing the number of degenerate electrons that provide such pressure before the neutrons themselves compensate the loss of pressure. For the isolated crust, the drip neutrons start from zero, since interpolation is used after the drip (see §2.2.1), contrary to the accreted crust where the first neutron number fraction beyond the drip is not zero. Therefore, the initial high value of P_n is seen in the plots.

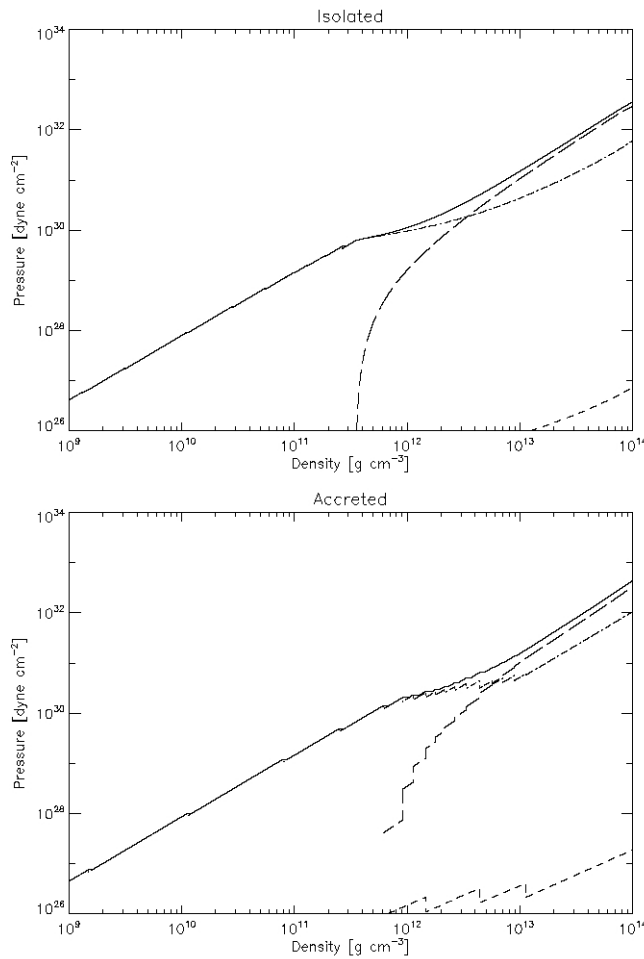


Figure 3.1: Pressure in the crust for isolated (*above*) and accreted compositions (*below*). We show the different contributors to the pressure such as the electrons (*dotted-dashed lines*), neutrons (*dashed*) and ions (*dotted*).

The pressure does not vary significantly for isolated and accreted crust.

We can see the comparison of these two pressure profiles in figure 3.2.

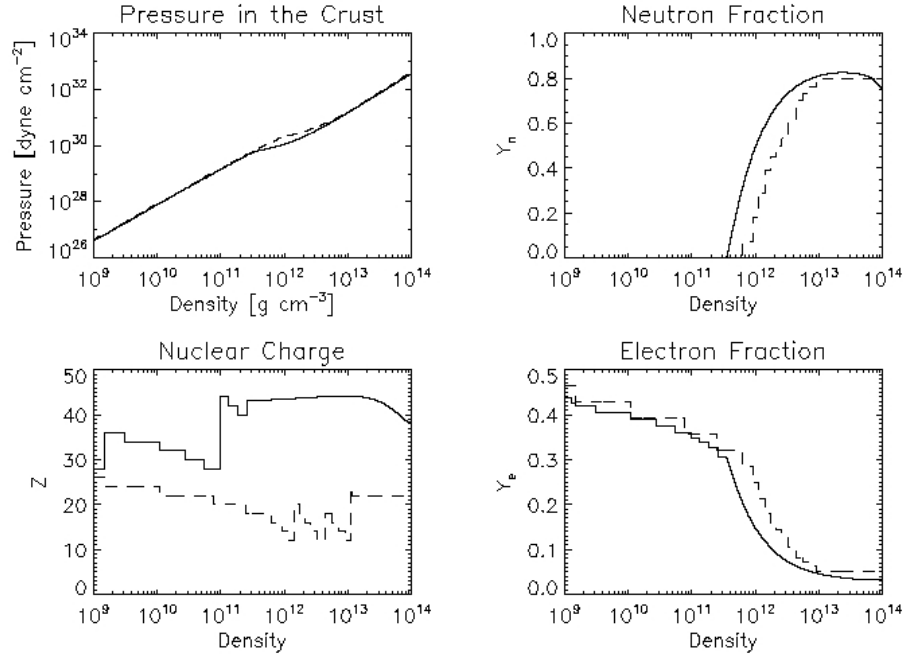


Figure 3.2: Pressure, neutron fraction Y_n , nuclear charge Z and electron charge Y_e for isolated (*solid*) and accreted (*dashed*) compositions

Conductivity

The conductivity profiles are obtained using the expression 2.32. Two plots obtained for K at different temperatures can be seen in the figure 3.3, for each composition. We can see that the value of the conductivity gets closer to each other as the temperature rises.

Neutrino emission

We calculate the neutrino emissivity using the fitting formula 2.45. In Figure 3.4 it is possible to see the sensitivity of Q_ν to temperature. The significant difference between the upper and lower figures will be crucial in determining the temperature profiles of the star, since low Q_ν is emitted when temperature

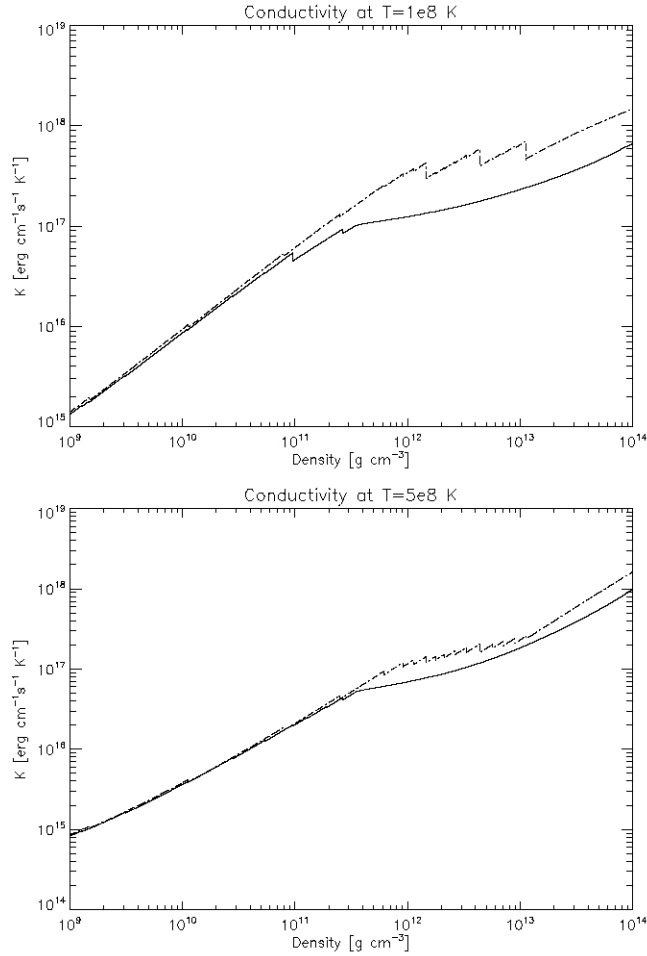


Figure 3.3: Thermal conductivity for isolated (*solid lines*) and accreted (*dashed-dotted lines*) compositions, for different constant temperatures in the crust, $T_c = 1 \times 10^8$ K (*upper figure*) and $T_c = 5 \times 10^8$ K (*below figure*).

is low ($\sim 10^8$ K). However this quantity can be significantly increased for small variations of T , reducing considerably the amount of heat that can be transferred by conduction. Although the first profile looks very different from the other two, in all three the same tendency (drop of Q_ν with density) is represented, although the density at which this drop occurs is much higher when temperature increases. We will see this further on when analyzing the solution of the structure equations. For this calculation we have only used the isolated composition.

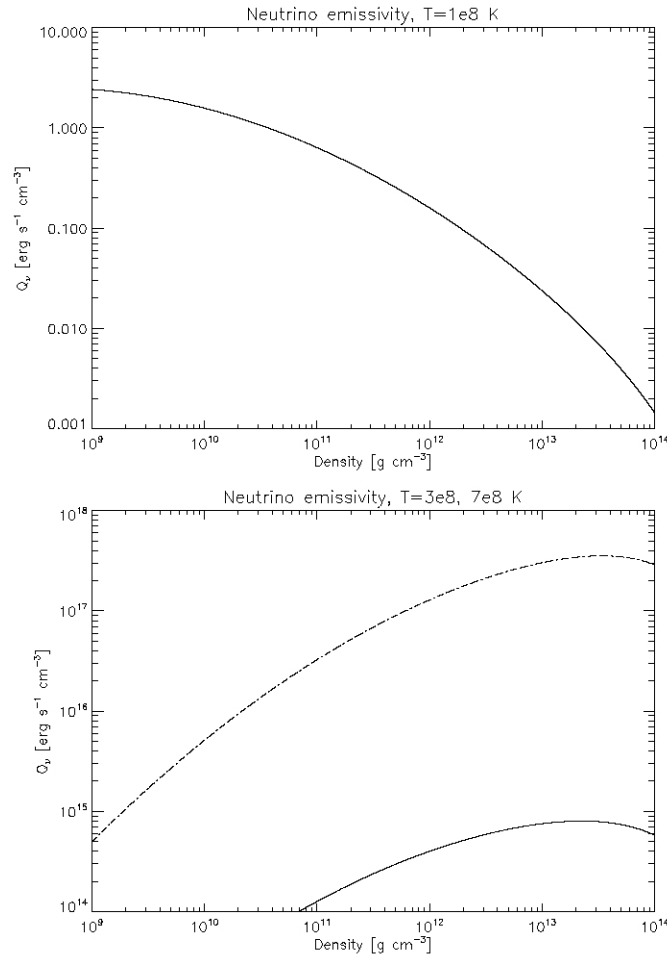


Figure 3.4: Neutrino emissivity Q_ν for different temperatures, in the upper figure $T = 1 \times 10^8$ K, and in the bottom one $T = 3 \times 10^8$ K (*solid*) and $T = 7 \times 10^8$ K (*dashed-dotted lines*).

Heat capacity

The heat capacity is only needed to calculate the thermal evolution of the star, so it is not necessary to show the steady-state thermal profile. However, we show the calculation only with the aim of illustrate its behaviour as another quantity that determines features of the crust.

To obtain the neutrino emissivity Q_ν we use the fitting formulas shown in eqs. 2.51 and 2.61, according to the condition of liquid ($\Gamma < 175$) or solid ($\Gamma > 175$) crust.

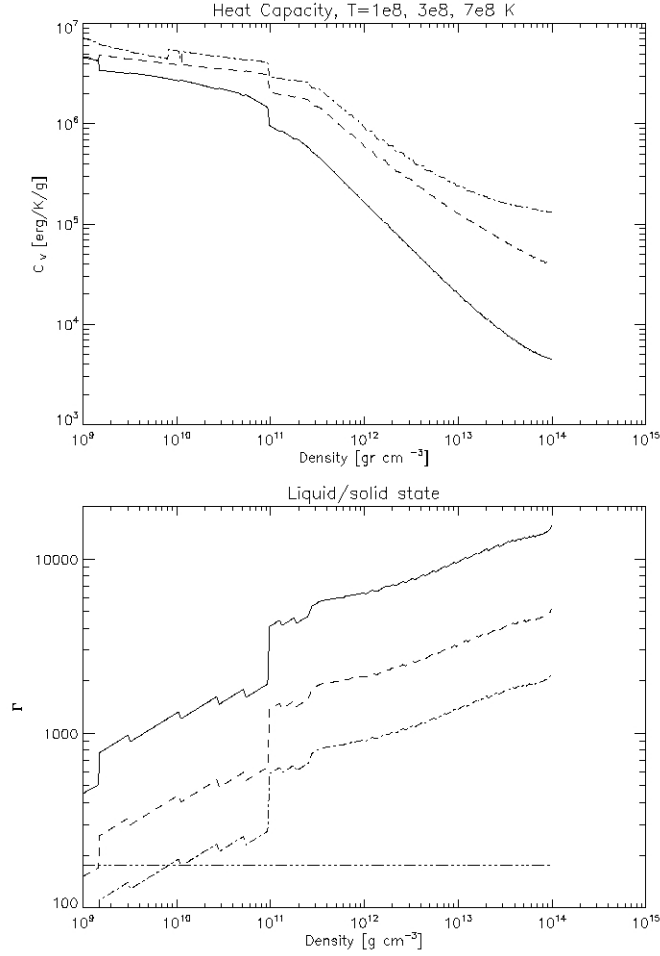


Figure 3.5: Heat Capacitance for different constant temperatures, $T_c = 1 \times 10^8$ (*solid*), $T_c = 3 \times 10^8$ (*dashed*) and $T_c = 7 \times 10^8$ (*dashed-dotted*). The horizontal line at $\Gamma = 175$ represents the phase change of the matter in the crust.

As we can see in the upper figure in 3.5, C_v increases with temperature, which becomes more evident for deep regions in the crust. The phase change is shown in the figure below. On the left of the same figure, when $T = 7 \times 10^8$ K it is possible to see the “ocean” part of the crust (liquid phase) as a smooth curve that drops down to $\rho \sim 1 \times 10^9$ g cm⁻³, when the crust becomes solid and C_v increases a small amount. The same occurs when $T = 3 \times 10^8$ K but for a smaller density region ($\sim 1 \times 10^9 - 2 \times 10^9$ g cm⁻³). For $T = 1 \times 10^8$ K

the crust is always solid.

After this brief summary of the behavior of the parameters we use to construct the steady-state model of the crust, we present the results for the solution of the structure equations.

§3.1.2 Results and Discussion

In the previous figures we have seen that the bottom and top of the crust have been set to $\rho_{bottom} = 10^9 \text{ g cm}^{-3}$ and $\rho_{top} = 10^{14} \text{ g cm}^{-3}$, respectively. As was pointed out in section §2.1, the bottom border was chosen slightly lower than density of nuclear matter saturation ($\rho = 2.8 \times 10^{14} \text{ g cm}^{-3}$). It was also indicated how the top border varies with temperature for accreted and isolated neutron stars. Therefore, we choose to set the top of the crust up to where it will extend for a wide range of surface temperatures, in accreted and isolated stars.

With this in mind, to integrate throughout the star interior, we use the change of variable from the expression 3.7. Hence, instead of using ρ , we will integrate throughout the column density. We get y from the hydrostatic equilibrium condition (eq. 3.3),

$$\frac{dP}{dy} = gy, \quad (3.9)$$

where $g = GM/R^2$. For the standard values of a neutron star, $M = 1.4 M_{\odot}$ and $R = 10^5 \text{ cm}$, $g = 1.857 \times 10^{14}$. Thus, we first calculate the pressure for a given density with the above equation to obtain y , within the range of densities $10^9 - 10^{14} \text{ g cm}^{-3}$.

The boundary conditions are set to flux and temperature at the top of the crust, integrating inwards. In the case of accreting neutron stars, we choose the initial flux in terms of $F_{out} = \dot{m}Q_{nuc}$ (Cumming et al., 2006), with an accretion rate of $\sim 10^4 \text{ g/cm}^2/\text{s}$ and the energy released per nucleon $Q_{nuc} \sim 10^{17} \text{ erg/g}$, so $F_{out} \simeq 10^{21} \text{ erg/cm}^2/\text{s}$. To set the temperature, considering different values from the literature —e.g. Brown (2000)— we use $T_{out} \sim 5 \times 10^8 \text{ K}$. Finally, in the flux equation from eq. 3.7 we take $\epsilon_{\nu} = \rho Q_{\nu}$.

We integrated the set of differential equations for a wide range of temperatures and fluxes around the two values mentioned above. We have chosen to show two sets of solutions in Figures 3.6 and 3.7. For the first figure we have used $F_{out} = 2 \times 10^{21}$ erg/cm²/s and three different temperatures $T_{out} = 1 \times 10^8$, 5×10^8 and 8×10^8 K. We found that lower initial fluxes (say $\sim 10^{20}$ erg/cm²/s and below) do not induce a significant change in the temperature profile, unless we choose the initial temperature larger as well (e.g. $\sim 10^9$ K for $F \sim 10^{20}$ erg/cm²/s). The composition data for an accreted neutron star have been used in the following solutions. Since the differences between this and isolated composition are not considerable (for the parameters considered here), we can restrict ourselves to the accreted case.

In the figures we can also see how the neutrino emissivity change along the column depth. Observe in Figure 3.6 the large differences between the values of ϵ_ν for the first ($T_{out} = 1 \times 10^8$ K) and the other two temperatures. This indicates the strong dependence of the neutrino emissivity for small variations of temperature, a variation of a factor of only 5 in temperature produces a difference of ~ 4 orders of magnitude in temperature. We can also see a slight increment of ϵ_ν at the bottom of the crust when $T_{out} = 8 \times 10^8$ K, which may account for the corresponding high flux. This suggest that, if neutrino losses are important, a much higher flux is necessary to sustain the temperature fixed at the top.

The flux profile, on the other hand, changes more appreciably. These results indicate that to achieve the value of F_{out} , the flux deep in the crust must increase considerably (when $T_{out} = 1 \times 10^8$ K, the flux is even almost constant). This accounts, of course, for the neutrino losses along the crust. This also suggests that if neutrino emissivity keeps increasing as on the profile for $T_{out} = 8 \times 10^8$ K, the flux in the crust will have to increase in order to compensate these ϵ_ν losses and maintain the thermal energy supply.

We also present the calculation for the heat capacity. As we said, this is shown just with the aim of illustrate another property that characterizes the crust. In Figure 3.6 we see how the overall profile of C_v does not change much along the crust. However, each curve reflects the strong dependence of C_v in composition (for clarity, we have only show C_v for two temperatures). We can

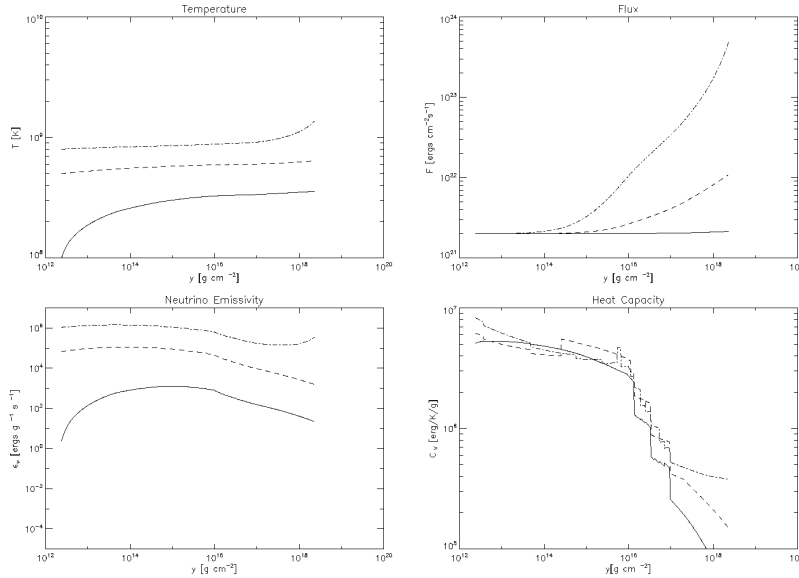


Figure 3.6: Temperature and Flux profiles for $F_{out} = 2 \times 10^{21}$ $\text{erg/cm}^2/\text{s}$ and three different initial temperatures $T_{out} = 1 \times 10^8$ K (*solid*), 3×10^8 K (*dashed*) and 8×10^8 K (*dotted-dashed*). The heat capacity C_v and neutrino emissivity ϵ_ν for this temperatures are also shown.

observe also a change of slope in these curves at the transition from liquid to solid material, for $T = 1 \times 10^8$ K the curve is continuous for almost half of the crust, while for the other two curves there is a “step” at the phase change.

The Figure 3.7 includes another set of solutions for the structure equations. Again, we set the flux value at the top of the crust ($F_{out} = 1 \times 10^{22}$ $\text{erg/cm}^2/\text{s}$) and integrate for three different temperatures $T_{out} = 1 \times 10^8$, 3×10^8 and 5×10^8 K, inwards in the crust. It is interesting to observe how the profiles get closer to each other as the column density increases in the crust. However, we have found that our code does not integrate temperatures over higher F_{out} ranges than the order of magnitude chosen here, unless the temperature at the top is lower (say $T_{out} \sim 10^7$ K). In this sense, the program is very sensitive to the election of high fluxes, and though this can be fixed by reducing the temperature, it does not necessarily represent the physical behaviour of the crust.

The neutrino emissivity, on the other hand, does not change significantly

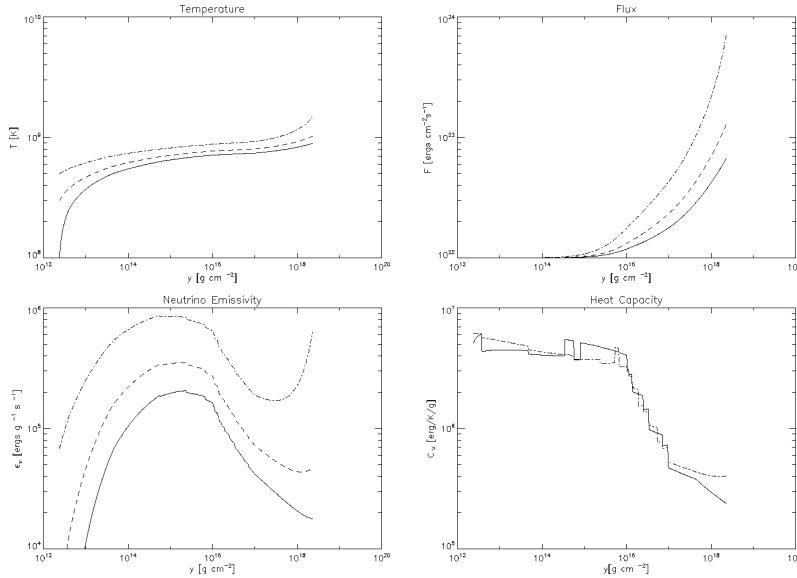


Figure 3.7: Temperature and Flux profiles for $F_{out} = 1 \times 10^{22}$ $\text{erg/cm}^2/\text{s}$ and three different initial temperatures $T_{out} = 1 \times 10^8$ K (*solid*), 3×10^8 K (*dashed*) and 5×10^8 K (*dotted-dashed*). We also show the profiles for neutrino emissivity ϵ_{nu} and heat capacity C_v , although for the latter only for the top and bottom temperatures (for clarity in the plot).

for the first two lowest temperatures, but it is noticeable how the emissivity rises again at the bottom of the crust when $T_{out} = 5 \times 10^8$ K, unlike at the other temperatures. Although this increment in ϵ_{ν} does not prevent the temperature from rising, we can see how the temperature profiles are close to each other for most of the crust. The heat capacity as in the previous solution, does not show an overall change but demonstrate features that reflect its composition dependence.

As we have said, we perform several integrations for wide ranges of flux and temperatures. The simulations have shown that for outgoing fluxes below $\sim 10^{20}$ $\text{erg/cm}^2/\text{s}$, neither the temperature profile nor the flux change appreciably. For the flux this is consistent with the behaviour of the neutrino emissivity, as we see in the Figure 3.7 ($T_{out} = 1 \times 10^8$ K), where lower temperatures correspond to a much lower ϵ_{nu} compared to those emissivities for temperatures a bit higher. We also perform simulations using outwards integration (from the bottom of the crust). The results were consistent with those

presented here (inwards integration).

§3.2 Conclusions

We have presented a simulation of a steady-state model of the neutron star crust. To this aim, we included a review of the observational phenomena where it is believed the crust plays an important role. We have also reviewed general characteristics of the crust within the context of the whole neutron star, considering the two main different scenarios where the neutron stars have been observed to exist, i.e. isolated and subjected to accretion processes.

The elements that conformed the steady-model have also been analyzed so we could present the calculations for each one in the context of the simulations. Finally the description of the method and the results are shown, which include the profiles of temperature and flux along the crust. We found that the behaviour of these two variables correspond to the expectations, considering the values used as boundary conditions. In spite of this, we have also mentioned that after pushing the initial values beyond certain quantity, we observed behaviour which does not seem to correspond to the nature of the crust. Nonetheless, the results obtained here appear to reflect the broad compartment of those parameters in the crust.

As has been said throughout this work, to construct models of the neutron star crust allow us to constrain, by means of observational data, the characteristics of the interior of these particular stars, which in turn represent a unique laboratory in the universe.

Our model intends to present a phenomenological analysis of the main physical quantities that govern observational features in the crust. It can be improved in many ways. Firstly, extending the model to a time-dependent simulation (using eq.3.5), mainly with the purpose of studying the cooling features of neutron stars. Secondly, we avoided the inclusion of some variables in the calculations, such as the *radiation pressure* or the possible reheating processes within the crust, that can ultimately be the main reason for the apparition of some phenomena (Kaminker et al., 2006). A more serious analysis would contemplate the inclusion of magnetic fields as well, since the cooling

processes in magnetars are obviously affected by them.

Bibliography

- ABE, R., 1959. Giant Cluster Expansion Theory and Its Application to High Temperature Plasma. *Progress of Theoretical Physics*, **22**, 213–226.
- ARRAS, P., CUMMING, A. & THOMPSON, C., 2004. Magnetars: Time Evolution, Superfluid Properties, and the Mechanism of Magnetic Field Decay. *Astrophysical Journal*, **608**, L49–L52.
- BAYM, G., PETHICK, C. & SUTHERLAND, P., 1971. The Ground State of Matter at High Densities: Equation of State and Stellar Models. *Astrophysical Journal*, **170**, 299–+.
- BROWN, E. F., 2000. Nuclear Heating and Melted Layers in the Inner Crust of an Accreting Neutron Star. *Astrophysical Journal*, **531**, 988–1002.
- CAMPANA, S., 2005. Variability in the Quiescent State of Neutron Star Transients. In F. A. Rasio & I. H. Stairs, eds., *Binary Radio Pulsars*, vol. 328 of *Astronomical Society of the Pacific Conference Series*, 291–+.
- CHABRIER, G., ASHCROFT, N. W. & DEWITT, H. E., 1992. White dwarfs as quantum crystals. *Nature*, **360**, 48–50.
- CHABRIER, G. & POTEKHIN, A. Y., 1998. Equation of state of fully ionized electron-ion plasmas. *Physical Review E*, **58**, 4941–+.
- COHEN, E. G. D. & MURPHY, T. J., 1969. New Results in the Theory of the Classical Electron Gas. *Physics of Fluids*, **12**(7), 1404–1411.

- CUMMING, A., ARRAS, P. & ZWEIBEL, E., 2004. Magnetic Field Evolution in Neutron Star Crusts Due to the Hall Effect and Ohmic Decay. *Astrophysical Journal*, **609**, 999–1017.
- CUMMING, A. & BILDSTEN, L., 2001. Carbon Flashes in the Heavy-Element Ocean on Accreting Neutron Stars. *Astrophysical Journal*, **559**, L127–L130.
- CUMMING, A. & MACBETH, J., 2004. The Thermal Evolution following a Superburst on an Accreting Neutron Star. *Astrophysical Journal*, **603**, L37–L40.
- CUMMING, A., MACBETH, J., IN 'T ZAND, J. J. M. & PAGE, D., 2006. Long Type I X-Ray Bursts and Neutron Star Interior Physics. *Astrophysical Journal*, **646**, 429–451.
- DEWITT, H. & SLATTERY, W., 1999. Screening enhancement of thermonuclear reactions in high density stars. *Contributions to Plasma Physics*, **39**, 97–100.
- DOUCHIN, F. & HAENSEL, P., 2001. A unified equation of state of dense matter and neutron star structure. *Astronomy and Astrophysics*, **380**, 151–167.
- GEPPERT, U., KUEKER, M. & PAGE, D., 2005. Temperature Distribution in Magnetized Neutron Star Crusts. In A. Baykal, S. K. Yerli, S. C. Inam & S. Grebenev, eds., *NATO ASIB Proc. 210: The Electromagnetic Spectrum of Neutron Stars*, 79–+.
- GRINDLAY, J. E., MCCLINTOCK, J. E., CANIZARES, C. R., COMINSKY, L., LI, F. K., LEWIN, W. H. G. & VAN PARADIJS, J., 1978. Discovery of optical bursts from an X-ray burst source, MXB1735-44. *Nature*, **274**, 567–+.
- GUPTA, S., BROWN, E. F., SCHATZ, H., MÖLLER, P. & KRATZ, K.-L., 2007. Heating in the Accreted Neutron Star Ocean: Implications for Superburst Ignition. *Astrophysical Journal*, **662**, 1188–1197.

- HAENSEL, P., 2001. Neutron Star Crusts. In D. Blaschke, N. K. Glendenning & A. Sedrakian, eds., *Physics of Neutron Star Interiors*, vol. 578 of *Lecture Notes in Physics*, Berlin Springer Verlag, 127–+.
- HAENSEL, P. & PICHON, B., 1994. Experimental nuclear masses and the ground state of cold dense matter. *Astronomy and Astrophysics*, **283**, 313–318.
- HAENSEL, P. & ZDUNIK, J. L., 1990a. Equation of state and structure of the crust of an accreting neutron star. *Astronomy and Astrophysics*, **229**, 117–122.
- HAENSEL, P. & ZDUNIK, J. L., 1990b. Non-equilibrium processes in the crust of an accreting neutron star. *Astronomy and Astrophysics*, **227**, 431–436.
- HAENSEL, P. & ZDUNIK, J. L., 2003. Nuclear composition and heating in accreting neutron-star crusts. *Astronomy and Astrophysics*, **404**, L33–L36.
- HOFFMAN, J. A., MARSHALL, H. L. & LEWIN, W. H. G., 1978. Dual character of the rapid burster and a classification of X-ray bursts. *Nature*, **271**, 630–633.
- KAMINKER, A. D., PETHICK, C. J., POTEKHIN, A. Y., THORSSON, V. & YAKOVLEV, D. G., 1999. Neutrino-pair bremsstrahlung by electrons in neutron star crusts. *Astronomy and Astrophysics*, **343**, 1009–1024.
- KAMINKER, A. D., YAKOVLEV, D. G., POTEKHIN, A. Y., SHIBAZAKI, N., SHTERNIN, P. S. & GNEDIN, O. Y., 2006. Magnetars as cooling neutron stars with internal heating. *Monthly Notices of the Royal Astronomical Society*, **371**, 477–483.
- KEEK, L., IN'T ZAND, J. J. M. & CUMMING, A., 2006. The superburst recurrence time in luminous persistent LMXBs. *Astronomy and Astrophysics*, **455**, 1031–1036.
- KEEK, L., IN'T ZAND, J. J. M., KUULKERS, E., CUMMING, A., BROWN, E. F. & SUZUKI, M., 2008. First superburst from a classical low-mass X-ray binary transient. *Astronomy and Astrophysics*, **479**, 177–188.

- KUULKERS, E., 2004. The observers' view of (very) long X-ray bursts: they are super! *Nuclear Physics B Proceedings Supplements*, **132**, 466–475.
- LANDAU, L. D. & LIFSHITZ, E. M., 1969. *Statistical physics. Pt.1*. Course of theoretical physics - Pergamon International Library of Science, Technology, Engineering and Social Studies, Oxford: Pergamon Press, and Reading: Addison-Wesley.
- LEWIN, W. H. G., CLARK, G. & DOTY, J., 1976. X-ray bursts. *International Astronomical Union Circulars*, **2922**, 1–+.
- LEWIN, W. H. G., VAN PARADIJS, J. & TAAM, R. E., 1993. X-Ray Bursts. *Space Science Reviews*, **62**, 223–389.
- LEWIN, W. H. G., VAN PARADIJS, J. & VAN DEN HEUVEL, E. P. J., 1997. *X-ray Binaries*. X-ray Binaries, Edited by Walter H. G. Lewin and Jan van Paradijs and Edward P. J. van den Heuvel, pp. 674. ISBN 0521599342. Cambridge, UK: Cambridge University Press, January 1997.
- MACKIE, F. & BAYM, G., 1977. Compressible liquid drop nuclear model and mass formula. *Nuclear Physics A*, **285**, 332–348.
- MARASCHI, L. & CAVALIERE, A., 1977. X-ray bursts of nuclear origin?. In *X-ray Binaries and Compact Objects*, 127–128.
- POTEKHIN, A. Y. & CHABRIER, G., 2000. Equation of state of fully ionized electron-ion plasmas. II. Extension to relativistic densities and to the solid phase. *Physical Review E*, **62**, 8554–8563.
- POTEKHIN, A. Y. & CHABRIER, G., 2000. Equation of state of fully ionized electron-ion plasmas. II. Extension to relativistic densities and to the solid phase. *Physical Review E*, **62**(6), 8554–8563.
- POTEKHIN, A. Y., CHABRIER, G. & YAKOVLEV, D. G., 1997. Internal temperatures and cooling of neutron stars with accreted envelopes. *Astronomy and Astrophysics*, **323**, 415–428.

- RUTLEDGE, R. E., BILDSTEN, L., BROWN, E. F., PAVLOV, G. G. & ZAVLIN, V. E., 2002. Variable Thermal Emission from Aquila X-1 in Quiescence. *Astrophysical Journal*, **577**, 346–358.
- SCHATZ, H., BILDSTEN, L., CUMMING, A. & WIESCHER, M., 1999. The Rapid Proton Process Ashes from Stable Nuclear Burning on an Accreting Neutron Star. *Astrophysical Journal*, **524**, 1014–1029.
- SHAPIRO, S. L. & TEUKOLSKY, S. A., 1983. *Black holes, white dwarfs, and neutron stars: The physics of compact objects*. New York, Wiley-Interscience, 1983, 663 p.
- THORNE, K. S., 1977. The relativistic equations of stellar structure and evolution. *Astrophysical Journal*, **212**, 825–831.
- USHOMIRSKY, G. & RUTLEDGE, R. E., 2001. Time-variable emission from transiently accreting neutron stars in quiescence due to deep crustal heating. *Monthly Notices of the Royal Astronomical Society*, **325**, 1157–1166.
- WACHTER, S., KOUVELIOTOU, C., PATEL, S., FIGER, D. & WOODS, P., 2007. Spitzer space telescope observations of SGR and AXP environments. *Astrophysics and Space Science*, **308**, 67–71.
- WIJNANDS, R., 2001. Recurrent Very Long Type I X-Ray Bursts in the Low-Mass X-Ray Binary 4U 1636-53. *Astrophysical Journal*, **554**, L59–L62.
- YAKOVLEV, D. G., GNEDIN, O. Y., KAMINKER, A. D. & POTEKHIN, A. Y., 2008. Theory of cooling neutron stars versus observations. In *40 Years of Pulsars: Millisecond Pulsars, Magnetars and More*, vol. 983 of *American Institute of Physics Conference Series*, 379–387.
- YAKOVLEV, D. G. & PETHICK, C. J., 2004. Neutron Star Cooling. *Annual Review of Astronomy and Astrophysics*, **42**, 169–210.